# A Modular System for Constructing Dynamical Systems

Isaac Freeman

6 March, 1998

## Abstract

This thesis discusses a method based on the dual principle of Rössler, and developed by Deng, for systematically constructing robust dynamical systems from lower dimensional subsystems. Systems built using this method may be modified easily, and are suitable for mathematical modelling.

Extensions are made to this scheme, which allow one to describe a wider range of dynamical behaviour. These extensions allow the creation of systems that reproduce qualitative features of the Lorenz Attractor (including bifurcation properties) and of Chua's circuit, but which are easily extensible.

# Contents

# List of Figures

# List of Tables

# Chapter 1

# Introduction

It is one thing to understand the features of a given dynamical system, but another to specify from scratch a system that exhibits a given set of features. Ideally, we would like to have a method for combining a collection of well-understood "standard parts", each of which describes a feature of the intended system, into a whole that retains the desired features of each part. It is further desirable that each part be largely independent of the others, so that modifications can be made to one part without effects on the rest of the system. Complicated systems could then be constructed like models built from LEGO™ bricks.

In 1976, the biochemist Rössler [Rös76] postulated a "dual principal" for building model dynamical systems. The idea was to separate the system into two subsystems, an "ordinary two-variable chemical oscillator" and an "ordinary single variable chemical hysteresis system". The former consists of various states in which the system spends most of its time, and the latter a mechanism for switching between those states. Rössler stated that "according to the same dual principle, many more analogous systems can be devised, no matter whether chemical, biochemical, biophysical, ecological, sociological, economic, or electronic in nature."

In order to implement this system, however, Rössler fell back on trial-and-error methods, and although he unexpectedly found a few interesting systems, including the Rössler attractor, the idea did not become popular.

In 1994, Bo Deng [Den94] published a more rigorously mathematical method for constructing systems using the Rössler dual principle. Rössler's "chemical oscillator" and "hysteresis system" are interpreted as slow and fast subsystems respectively which can be constructed separately and used as building blocks. The resulting dynamical systems are robust, and amenable to modification in clear and simple ways. Discussion in this thesis is confined to three-dimensional examples, but the method developed by Deng can be applied to $n$-dimensional systems.

This thesis uses a modification of Deng's scheme to make models that reproduce the behaviour of strange attractors found in two important nonlinear dynamical systems: that of Lorenz (the famous "butterfly attractor") and Chua's circuit (the Double Scroll Attractor).

Chapter 2 introduces the method for modelling dynamical systems developed by Deng, and presents a number of examples. Those in sections 2.3.1 to 2.3.4 inclusive are due to Deng, and the remainder to the present author. This chapter also discusses the role of timing constants.

In chapter 3 a model is built that describes the Lorenz system, for which extensions are required to Deng's scheme.

Chapter 4 describes a model of the Chua system.
Chapter 5 is the conclusion.

# Chapter 2

# Deng's Scheme

## 2.1 Sectioning a dynamical system

We can divide a multidimensional dynamical system into lower dimensional subsystems by taking sections at constant values of a selected variable, and describing the flows projected onto each of the sections. As more sections are added, the behaviour will approach the behaviour of the globally-defined system.

For a simple sectioning of a three-dimensional system with $n$ horizontal planes, each with constant $z$, these equations would have a form as follows:

$$
\begin{aligned}
\dot{x} &= (z-z_2)(z-z_3)\ldots(z-z_n)f_{1_x}(x,y) \\
&+ (z-z_1)(z-z_3)\ldots(z-z_n)f_{2_x}(x,y) \\
&+ (z-z_1)(z-z_2)(z-z_4)\ldots(z-z_n)f_{3_x}(x,y) \\
&\vdots \\
&+ (z-z_1)(z-z_2)\ldots(z-z_{n-1})f_{n_x}(x,y) \\
\dot{y} &= (z-z_2)(z-z_3)\ldots(z-z_n)f_{1_y}(x,y) \\
&+ (z-z_1)(z-z_3)\ldots(z-z_n)f_{2_y}(x,y) \\
&+ (z-z_1)(z-z_2)(z-z_4)\ldots(z-z_n)f_{3_y}(x,y) \\
&\vdots \\
&+ (z-z_1)(z-z_2)\ldots(z-z_{n-1})f_{n_y}(x,y) \\
\dot{z} &= (z-z_2)(z-z_3)\ldots(z-z_n)f_{1_z}(x,y) \\
&+ (z-z_1)(z-z_3)\ldots(z-z_n)f_{2_z}(x,y) \\
&+ (z-z_1)(z-z_2)(z-z_4)\ldots(z-z_n)f_{3_z}(x,y) \\
&\vdots \\
&+ (z-z_1)(z-z_2)\ldots(z-z_{n-1})f_{n_z}(x,y)
\end{aligned}
\tag{2.1}
$$

Thus, when $z = z_1$, all but one of the first of the terms in each equation disappears, and the system reduces to

$$
\begin{aligned}
\dot{x} &= (z_1-z_2)(z_1-z_3)\ldots(z_1-z_n)f_{1_x}(x,y) \\
\dot{y} &= (z_1-z_2)(z_1-z_3)\ldots(z_1-z_n)f_{1_y}(x,y) \\
\dot{z} &= (z_1-z_2)(z_1-z_3)\ldots(z_1-z_n)f_{1_z}(x,y)
\end{aligned}
\tag{2.2}
$$

so that the equations $f_{1_x}$, $f_{1_y}$, and $f_{1_z}$ describe the behaviour on the section $z = z_1$, up to the constant $(z_1 - z_2)(z_1 - z_3) \ldots (z_1 - z_n)$. Similarly, for each section $m$, there are corresponding equations $f_{m_x}$, $f_{m_y}$, and $f_{m_z}$ describing the behaviour of the system on that section.

At points between the sections, the functions $f_1 \ldots f_n$ weight the contributions of each term of the equation, so that the trajectory is always most strongly influenced by the behaviour on the closest sections. In order to accurately describe the effects of fixed points in the system, we must ensure that sections are chosen so that each fixed point lies on a section.

### 2.1.1 Example: a closed orbit

The equations

$$
\begin{aligned}
\dot{x} &= (z-1)z(z+1)(z+2)f_{1_x} \\
&\quad +(z-2)(z-1)z(z+1)f_{2_x} \\
&\quad +(z-2)(z-1)(z+1)(z+2)f_{3_x} \\
&\quad +(z-2)z(z+1)(z+2)f_{4_x} \\
&\quad +(z-2)(z-1)z(z+2)f_{5_x} \\
\dot{y} &= (z-1)z(z+1)(z+2)f_{1_y} \\
&\quad +(z-2)(z-1)z(z+1)f_{2_y} \\
&\quad +(z-2)(z-1)(z+1)(z+2)f_{3_y} \\
&\quad +(z-2)z(z+1)(z+2)f_{4_y} \\
&\quad +(z-2)(z-1)z(z+2)f_{5_y} \\
\dot{z} &= (z-1)z(z+1)(z+2)f_{1_z} \\
&\quad +(z-2)(z-1)z(z+1)f_{2_z} \\
&\quad +(z-2)(z-1)(z+1)(z+2)f_{3_z} \\
&\quad +(z-2)z(z+1)(z+2)f_{4_z} \\
&\quad +(z-2)(z-1)z(z+2)f_{5_z}
\end{aligned}
\tag{2.3}
$$

where

$$
\begin{aligned}
f_{1_x} &= \frac{1}{24} \\
f_{2_x} &= \frac{-1}{24} \\
f_{3_x} &= 0 \\
f_{4_x} &= \frac{-1}{6} \\
f_{5_x} &= \frac{1}{6} \\
f_{1_y} &= \frac{-y}{24} \\
f_{2_y} &= \frac{-y}{24} \\
f_{3_y} &= \frac{-y}{4} \\
f_{4_y} &= \frac{y}{6} \\
f_{5_y} &= \frac{y}{6}
\end{aligned}
$$

9
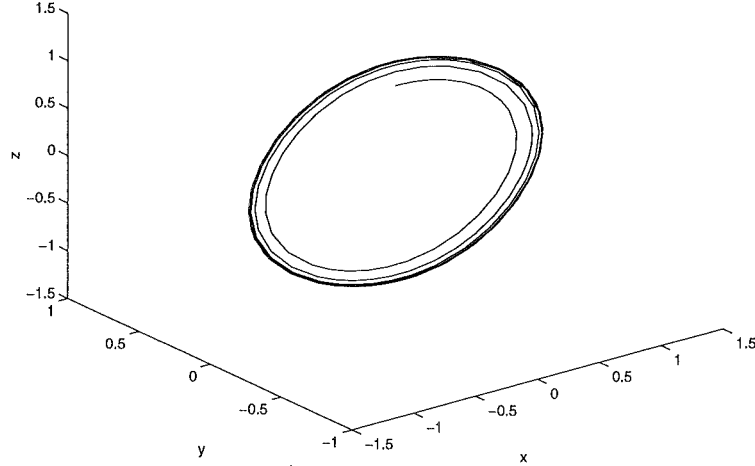
Figure 2.1: An attracting orbit defined in sections in equations 2.3

$$f_{1_z} = \frac{-1}{24}$$

$$f_{2_z} = \frac{1}{24}$$

$$f_{3_z} = \frac{-x}{4}$$

$$f_{4_z} = \frac{x}{6}$$

$$f_{5_z} = \frac{x}{6} \tag{2.4}$$

define a system with an attracting closed orbit of unit radius, shown in figure 2.1.

## 2.2 Fast and slow subsystems

This method tends to result in cumbersome equations, with much information duplicated. It would be desirable to reduce the number of sections to a minimum. Deng's version of the Rössler principle achieves this, by breaking the system into two parts: a 'slow' subsystem made of those attracting sections on which the system spends most of its time, and a 'fast' subsystem which describes the manner in which trajectories may switch from one section to another.

Under this scheme, the sections of the slow subsystem are not completely invariant, since trajectories on those sections are able eventually to switch to other sections. But the fast subsystem can be arranged so that the sections of the slow subsystem are largely stable, and the dynamics on them can closely approximate what would be the case if they were invariant.

### 2.2.1 Abstract Form

Deng specified forms for a three-dimensional system, with stable sections parallel to the $xy$-plane and fast subsystem acting in the $z$-direction as:

$$\dot{x} = f(x, y, z, \varepsilon)$$

10

$$\dot{y} = g(x,y,z,\varepsilon)$$

$$\varepsilon\dot{z} = h(x,y,z,\varepsilon) \tag{2.5}$$

where, on $\varepsilon = 0$,

$$
\begin{aligned}
f(x,y,z,0) &= (z-z_2)(z-z_3)\ldots(z-z_n)f_1(x,y) \\
&+ (z-z_1)(z-z_3)\ldots(z-z_n)f_2(x,y) \\
&+ \vdots \\
&+ (z-z_1)(z-z_2)\ldots(z-z_{n-1})f_n(x,y) \\
g(x,y,z,0) &= (z-z_2)(z-z_3)\ldots(z-z_n)g_1(x,y) \\
&+ (z-z_1)(z-z_3)\ldots(z-z_n)g_2(x,y) \\
&+ \vdots \\
&+ (z-z_1)(z-z_2)\ldots(z-z_{n-1})g_n(x,y) \\
h(x,y,z,0) &= (z-z_1)(z-z_2)\ldots(z-z_n)p(x,y,z) \tag{2.6}
\end{aligned}
$$

Here $z_1\ldots z_n$ are constants and $f_{1\ldots n}$, $g_{1\ldots n}$ and $p$ are polynomials. Thus the slow subsystem has $n$ 'branches' or sections for each of $z = z_1,\ldots,z = z_n$.

We choose the polynomial $p$ in (2.6) so that the the branches of the slow subsystem are asymptotically attracting in the fast subsystem. On the branches the behaviour of the system is completely determined by the choice of $f_1\ldots f_n$ and $g_1\ldots g_n$.

The parameter $\varepsilon$ controls switching between the branches. For $\varepsilon = 0$, the branches are invariant under the flow, and trajectories starting close to either branch will stay on that branch. For $\varepsilon > 0$, the intersections of the nullclines of $z$ bifurcate, creating gaps in the branches of the slow subsystem. With an appropriate choice of $p$, trajectories passing through those gaps can be directed to move between the branches of the slow subsystem. The fast subsystem acts as a switch, specifying where the flow can jump from one state (or branch of the slow manifold) to another.

In general, we have $0 < \varepsilon \ll 1$, so that the behaviour of the system is dominated by the slow subsystem, and the branches remain asymptotically attracting for all but small areas. In this situation, we can consider the flows on the branches of the slow subsystem independently of the fast subsystem, providing the desired 'modular' behaviour.

## 2.3  Examples

### 2.3.1  Systems with Z-Switches

**The Z-Switch**

A Z-switch is a fast subsystem of the form:

$$\varepsilon\dot{z} = (4-z^2)[z+2-m(x+2)] - \varepsilon cz \tag{2.7}$$

The name comes from the arrangement of the system's $z$-nullclines, which are given by the roots of the polynomial equation $h(x,y,z,\varepsilon) = 0$. For the Z-switch

$$h(x,y,z,\varepsilon) = (4-z^2)[z+2-m(x+2)] - \varepsilon cz \tag{2.8}$$

11
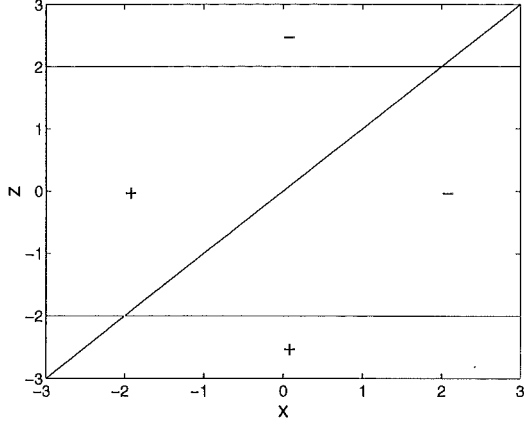
Figure 2.2: Nullclines of $z$ for the Z-switch with $\varepsilon = 0$. $+$ and $-$ symbols indicate the sign of $\dot{z}$ in various regions.
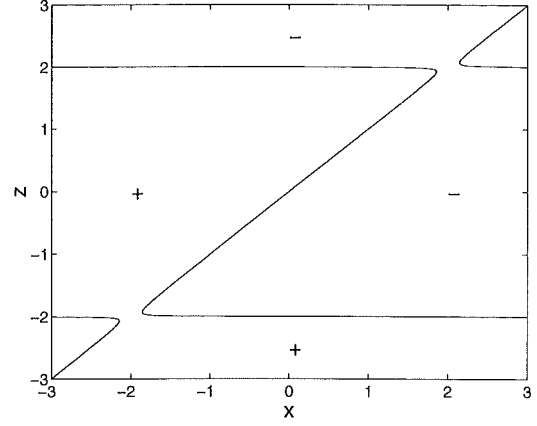
Figure 2.3: Nullclines of $z$ for the Z-switch with $\varepsilon > 0$. $+$ and $-$ symbols indicate the sign of $\dot{z}$ in various regions.

so that the nullclines are dependent on the value of the singular parameter $\varepsilon$. On $\varepsilon = 0$, $h(x,y,z,0) = 0$ the nullclines are $z = \pm 2$ and $z + 2 - m(x + 2) = 0$, as shown in figure 2.2. Note that the signs of $\dot{z}$ in various regions of the plane indicate that a flow will be attracted to $z = \pm 2$, where the two branches of the slow subsystem will be situated.

For $0 < \varepsilon \ll 1$, the intersection points of the three planes bifurcate, forming three connected components, one of which is the Z-shaped hysteresis that gives the switch its name. Figure 2.3 depicts this situation. Note the gaps in the $z = \pm 2$ branches. Any trajectory on the top branch that passes into this gap will drop down to the lower branch due to the sign of $\dot{z}$ in this region. Similarly, trajectories on the bottom branch may pass through the gap and switch to the top branch. For larger values of $\varepsilon$, the gaps become more pronounced.

**Shil'nikov's saddle-focus homoclinic orbit**

This system, first described by Shil'nikov [Shi70], has a single fixed point, a saddle, at $(2, 0, -2)$. The linearization of the vector field at the saddle has eigenvalues $\lambda \pm i\omega, \mu$ where $0 < \lambda < -\mu, \omega \neq 0$, and a homoclinic orbit links the stable and unstable manifolds. A strange attractor is evident when trajectories are plotted.

The following equations define a system that has such an orbit.

$$\begin{aligned}
\dot{x} &= -(z + 2)d(x - a) \\
&\quad +(2 - z)[\alpha(x - 2) - \beta y - \alpha(x - 2)\frac{(x - 2)^2 + y^2}{R^2}] \\
\dot{y} &= -(z + 2)(y - b) \\
&\quad +(2 - z)[\beta(x - 2) - \alpha y - \alpha(x - 2)\frac{(x - 2)^2 + y^2}{R^2}] \\
\varepsilon\dot{z} &= (4 - z^2)[z + 2 - m(x + 2)] - \varepsilon c z
\end{aligned} \tag{2.9}$$

Substituting $\varepsilon = 0, z = 2$ into the system of equations gives the reduced slow subsystem on the upper branch:

$$\begin{aligned}
\dot{x} &= -4d(x - a) \\
\dot{y} &= -4(y - b)
\end{aligned} \tag{2.10}$$

12
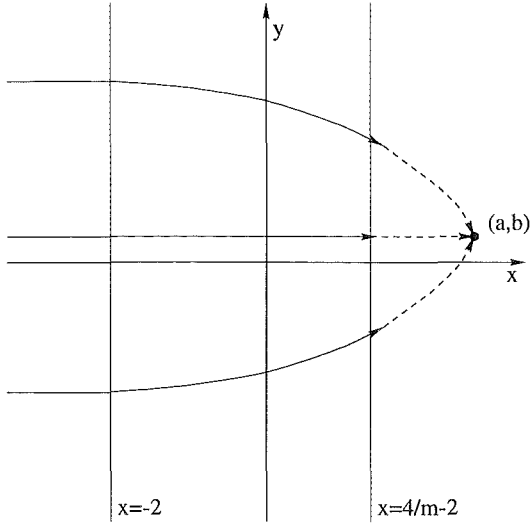
Figure 2.4: Phase portrait for the reduced slow subsystem (equations 2.10) on the $z = 2$ branch.
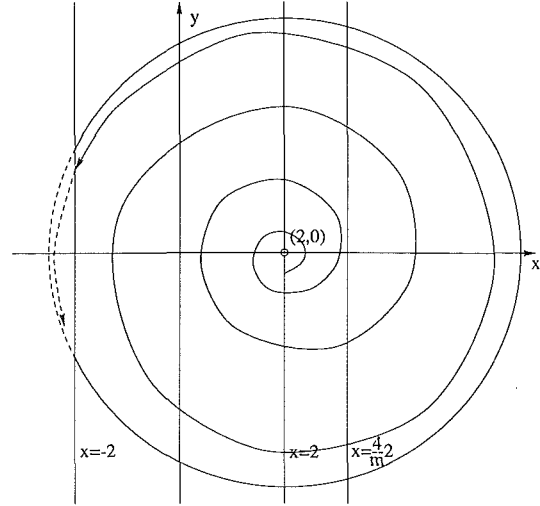
Figure 2.5: Phase portrait for the reduced slow subsystem (equations 2.11) on the $z = -2$ branch.

$$\dot{z} = 0$$

For $d > 0$, $a > \frac{4}{m} - 2$, every trajectory from the left of $x = \frac{4}{m} - 2$ moves to the right until it reaches the top turning points of the z-switch, $x = \frac{4}{m} - 2$ (see Figure 2.4). For $\varepsilon \neq 0$, the intersections of the $z$-nullclines bifurcate. At the turning points, the $z = 2$ phase plane is no longer invariant, and the trajectory is influenced by the fast subsystem. It quickly drops to the region of the lower $z = -2$ branch.

On the lower branch, the system of equations reduces to:

$$
\begin{aligned}
\dot{x} &= 4[\alpha(x-2) - \beta y - \alpha(x-2)\frac{(x-2)^2 + y^2}{R^2}] \\
\dot{y} &= 4[\beta(x-2) - \alpha y - \alpha(x-2)\frac{(x-2)^2 + y^2}{R^2}] \\
\dot{z} &= 0
\end{aligned}
\tag{2.11}
$$

or, in polar coordinates with origin at (2,0),

$$
\begin{aligned}
\dot{r} &= 4\alpha r(1 - \frac{r^2}{R^2}) \\
\dot{\theta} &= \beta
\end{aligned}
$$

For $\alpha > 0$ and $R > 2$, this branch of the subsystem has a repelling equilibrium point at the origin and an attracting periodic orbit $r = R$. A trajectory on this branch spirals out towards the attracting orbit until it meets the bottom turning points of the Z-switch at $x = z = -2$ (see Figure 2.5). At the turning points the trajectory makes an upward turn, jumping to the upper branch. The fixed point (2,0,-2) is hyperbolic. Figure 2.6 shows a trajectory on this system. A strange attractor is evident.

**Double spiral attractor**

This attractor shares most features with the Shil'nikov attractor - the fast subsystem is the same, and the terms describing the flow on the lower branch of the slow subsystem are

13
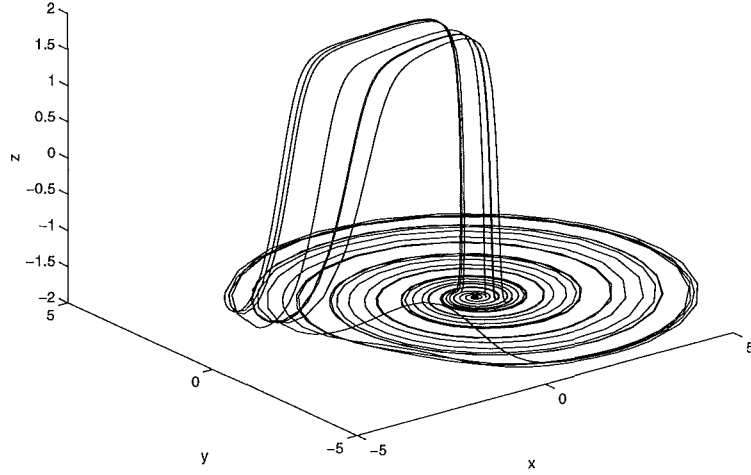
Figure 2.6: Shil'nikov attractor from equations 2.9, with $a = 7$, $b \doteq 1.435$, $c = 1$, $d = 1.5$, $m = 1.543$, $R = 6$, $\alpha = 0.5$, $\beta = 4$ and $\varepsilon = 0.08$

retained. The terms for the upper branch are modified, to create a second saddle with similar eigenvalues to the lower one. The trajectory now follows a spiral path on both the upper and lower branches.

$$
\begin{aligned}
\dot{x} &= (z+2)[\lambda(x-k) - \mu y - \lambda(x-k)\frac{(x-k)^2 + y^2}{R^2}] \\
&\quad +(2-z)[\alpha(x-2) - \beta y - \alpha(x-2)\frac{(x-2)^2 + y^2}{R^2}] \\
\dot{y} &= (z+2)[\mu(x-k) + \lambda y - \lambda y\frac{(x-k)^2 + y^2}{R^2}] \\
&\quad +(2-z)[\beta(x-2) - \alpha y - \alpha(x-2)\frac{(x-2)^2 + y^2}{R^2}] \\
\varepsilon\dot{z} &= (4-z^2)[z+2 - m(x+2)] - \varepsilon c z
\end{aligned}
\tag{2.12}
$$

Figure 2.7 shows an attractor generated from this system, with $\mu > 0$, and figure 2.8 an attractor with $\mu < 0$. Note that for $\mu > 0$, both branches spiral in an anti-clockwise direction, whereas for $\mu < 0$ they spiral in opposite directions.

**Twisted and non-twisted homoclinic orbits**

In a twisted homoclinic orbit, either the stable or unstable manifold is twisted like a Möbius strip. In a non-twisted orbit the manifold looks like a cylindrical band. The system below exhibits both behaviours, depending on the value of the parameter $d$.

$$
\begin{aligned}
\dot{x} &= (2-z)a(x-2) \\
&\quad +(z+2)[\alpha(x-x_0) + \beta(y-y_0)] \\
\dot{y} &= (2-z)[d(b-a)(x-2)/4 + by] \\
&\quad +(z+2)[-\beta(x-x_0) + \alpha(y-y_0)] \\
\varepsilon\dot{z} &= (2-z)(2+z)[z+2 - m(x+2)] - \varepsilon c z
\end{aligned}
\tag{2.13}
$$

14
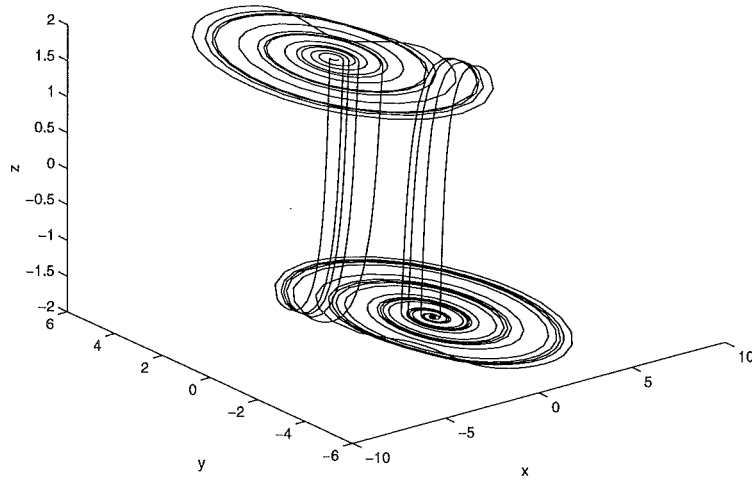
Figure 2.7: Co-directional double spiral attractor from equations 2.12 with $a = 7, b = 1.435, c = 1, m = 1.543, k = -3.4, R = 6, \alpha = 0.5, \beta = 4, \lambda = 0.5, \mu = 4$ and $\varepsilon = 0.08$
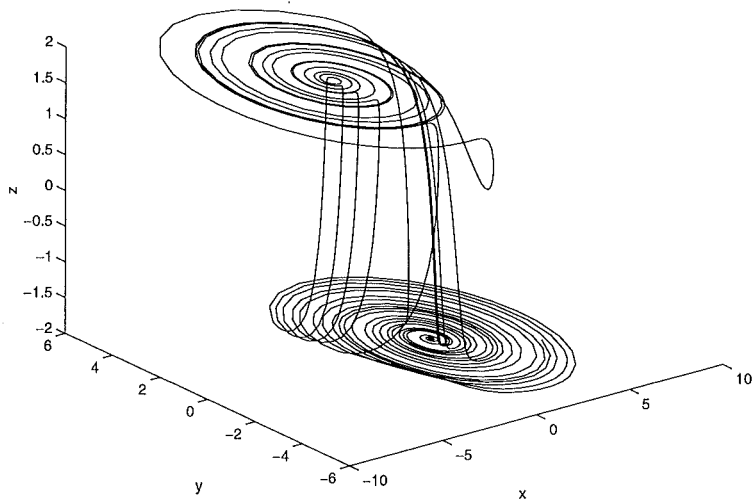


Figure 2.8: Oppositely-directed double spiral attractor from equations 2.12 with $a = 7, b = 1.435, c = 1, m = 1.543, k = -3.3, R = 6, \alpha = 0.5, \beta = 4, \lambda = 0.5, \mu = -4$ and $\varepsilon = 0.08$

15
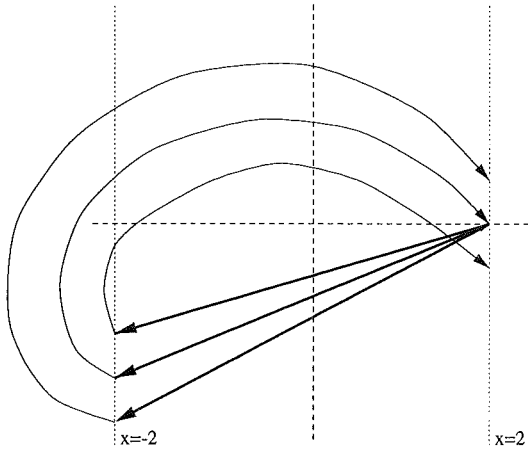
Figure 2.9: Phase portraits for the reduced slow subsystem of 2.13, with the value of $d$ chosen so that the homoclinic orbit is twisted. The heavy curves are trajectories on the lower $z = -2$ branch, and the lighter curves are trajectories on the upper $z = 2$ branch. The lines $x = -2$ and $x = 2$ are respectively the top and bottom turning edges.
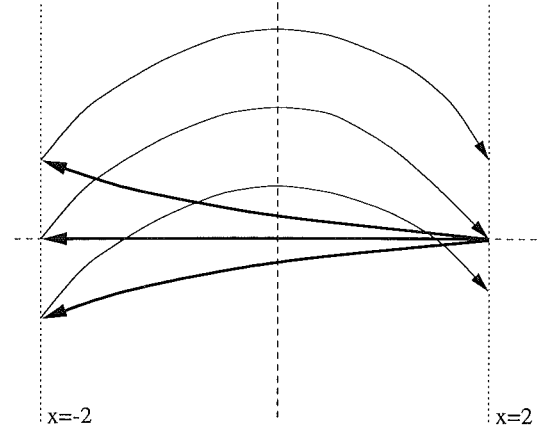
Figure 2.10: Phase portraits for the reduced slow subsystem of 2.13, with the value of $d$ chosen so that the homoclinic orbit is non-twisted. The heavy curves are trajectories on the lower $z = -2$ branch, and the lighter curves are trajectories on the upper $z = 2$ branch. The lines $x = -2$ and $x = 2$ are respectively the top and bottom turning edges.

Figures 2.9 and 2.10 show the flows on the upper and lower branches of the slow subsystem, for $a,b > 0$. On the lower branch the slow subsystem reduces to

$$\dot{x} = 4a(x-2)$$
$$\dot{y} = d(b-a)(x-2) + 4by$$

$$(2.14)$$

so that the linearization of the single fixed point at $(2, 0, -2)$ has eigenvalues $4a$ and $4b$, with corresponding eigenvectors $[4, -d]$ and $[0, 1]$ respectively. For $a > b$, $[4, -d]$ is the principal unstable eigenvector. Trajectories starting near the fixed point will roughly follow this eigenvector until they reach the $x = -2$ turning edge. The value of $d$ determines the value of $y$ at which trajectories hit the turning edge. On the upper branch of the slow subsystem, trajectories follow a spiral centred at $(x_0, y_0)$, until they hit the $x = 2$ turning edge, where they drop back to the lower branch. Depending on their $y$ position, the orientation of trajectories will either be preserved or reversed by the time they reach $x = 2$.

Figures 2.11 and 2.12 show trajectories close to twisted and untwisted orbits respectively.

### 2.3.2 Systems with Toroidal Switches

A toroidal switch is a fast subsystem of the form:

$$h(x,y,z,\varepsilon) = z(2-z)[z + m(x^2 + y^2) - h] - \varepsilon c(z-1) \quad (2.15)$$

The nullclines of $z$ for $\varepsilon = 0$ are shown in figure 2.13. The shape is similar to that of the Z-Switch except that the line $z+2-m(x+2) = 0$ is replaced with the paraboloid $z+m(x^2+y^2)-h = 0$,

16
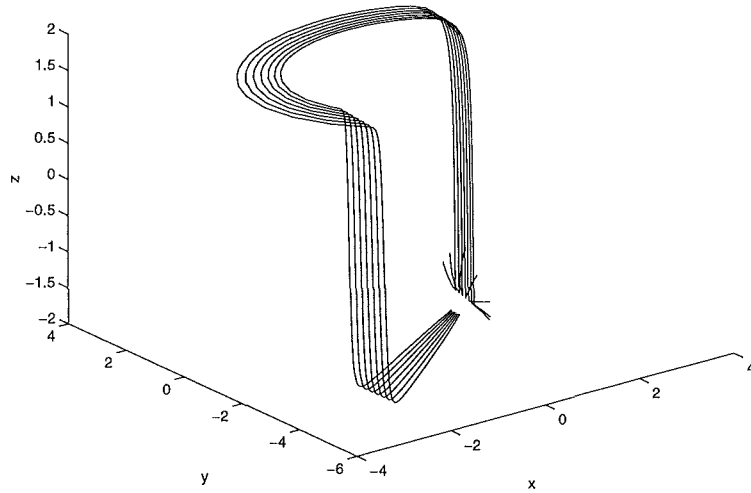
Figure 2.11: Several trajectories close to a twisted homoclinic orbit from equations 2.13, with $a = 1.5, b = 1, c = 2, d = 3.5, m = 1.1845, \alpha = 0.01, \beta = 5, x_0 = -0.1, y_0 = -2$ and $\varepsilon = 0.01$
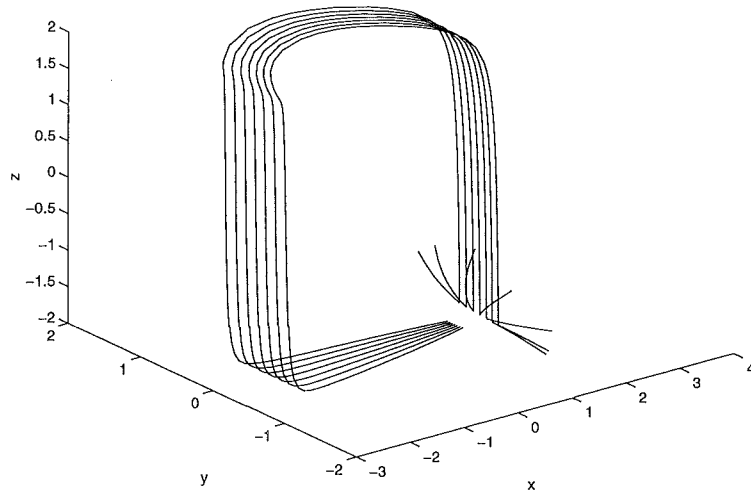


Figure 2.12: Several trajectories close to a non-twisted homoclinic orbit from equations 2.13, with $a = 1.5, b = 1, c = 2, d = -0.2, m = 1.1845, \alpha = 0.01, \beta = 5, x_0 = -0.1, y_0 = -2$ and $\varepsilon = 0.01$
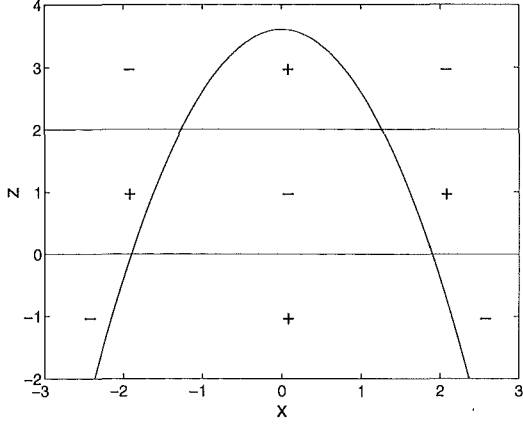
Figure 2.13: Nullclines of $z$ for the toroid switch with $\varepsilon = 0$ + and − symbols indicate the sign of $\dot{z}$ in various regions.
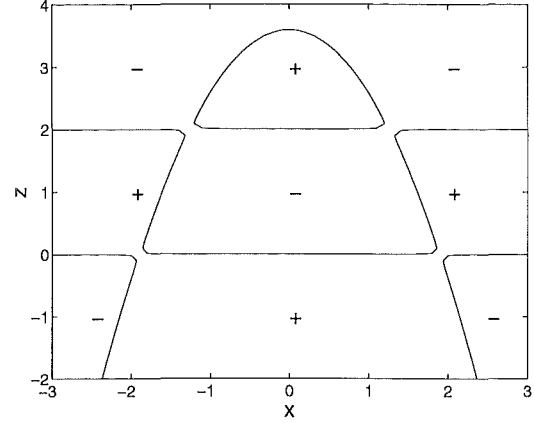
Figure 2.14: Nullclines of $z$ for the toroid switch with $\varepsilon > 0$ + and − symbols indicate the sign of $\dot{z}$ in various regions.

resulting in a switch that is rotationally symmetric about the $z$-axis. As before, the signs of $\dot{z}$ are such that the two branches of the slow subsystem, $z = 0$ and $z = 2$ are attracting.

On $\varepsilon > 0$, the turning edges will occur where the nullclines intersect, on the circles $x^2 + y^2 = h/m - 2$ and $x^2 + y^2 = h/m$.

In order to create periodic orbits or strange attractors using the toroid switch, we require a system with a repelling fixed point on the lower branch, so that trajectories move outwards to meet the lower turning circle, and an attracting fixed point on the upper branch so that trajectories move inwards towards the upper turning circle.

### 2.3.3 Invariant Toroid

A simple attracting orbit can be created on the toroid switch as shown in the following system:

$$
\begin{aligned}
\dot{x} &= z(\lambda x - \mu y) \\
&\quad + (2 - z)[\alpha x - \beta y - \alpha x \frac{x^2 + y^2}{R^2}] \\
\dot{y} &= z(\mu x + \lambda y) \\
&\quad + (2 - z)[\beta x + \alpha y - \alpha y \frac{x^2 + y^2}{R^2}] \\
\varepsilon \dot{z} &= z(2 - z)[z + m(x^2 + y^2) - h] - \varepsilon c(z - 1)
\end{aligned}
\tag{2.16}
$$

Figure 2.15 shows a trajectory on this orbit, exhibiting a toroid attractor.

The non-chaotic nature of this system is a result of several special arrangements. The reduced flows on the branches of the slow subsystem are both circular spirals, with fixed points aligned on the z axis. The top and bottom branches are parallel planes, and the paraboloid nullcline is rotationally symmetric about the z-axis. Breaking any of these symmetries will produce a chaotic attractor, as shown in the following examples.

**Folded Tori**

In the first example, we change the toroid switch so that the upper and lower branches are no longer parallel planes. This could be achieved by simply tilting the upper branch, but instead

18
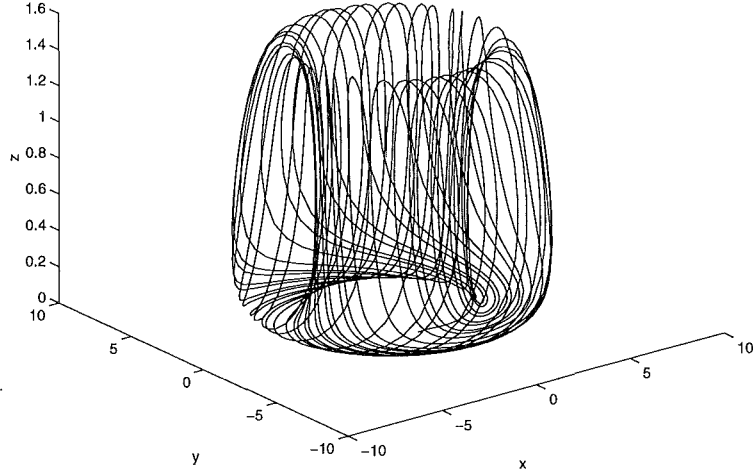
Figure 2.15: Invariant toroid attractor from equations 2.16, with $m = 0.1, h = 3.6, c = 1, R = 10, \lambda = -4, \mu = 2, \alpha = 2$ and $\beta = 3.0005$

we introduce a fold by replacing the factor $(2-z)$ in fast subsystem by $(2-z)[a(z-2)^2+b]-dx$, as shown in figures 2.16 and 2.17. In this case we choose values for the parameters $a, b$ and $d$ to create only a slight fold. In section 2.3.4 we discuss the effects of more extreme folding.

The modified toroid system is:

$$
\begin{aligned}
\dot{x} &= z(\lambda x - \mu y) \\
&\quad + (2-z)[\alpha x - a\beta y - \alpha x \frac{x^2 + y^2}{R^2}] \\
\dot{y} &= z(\mu x + \lambda y) \\
&\quad + (2-z)[\beta x + \alpha y - \alpha y \frac{x^2 + y^2}{R^2}] \\
\varepsilon \dot{z} &= z[(2-z)[a(z-2)^2 + b] - dx][z + m(x^2 + y^2) - h] - \varepsilon c(z-1)
\end{aligned}
\tag{2.17}
$$

Figure 2.18 shows the attractor.

In the second example, we return to the original toroid switch, but replace the circular spiral on the lower branch of the invariant toroid system with an elliptical spiral. We do this by simply introducing a new parameter $a$ into equations 2.16:

$$
\begin{aligned}
\dot{x} &= z(\lambda x - \mu y) \\
&\quad + (2-z)[\alpha x - a\beta y - \alpha x \frac{x^2 + y^2}{R^2}] \\
\dot{y} &= z(\mu x + \lambda y) \\
&\quad + (2-z)[\beta x + \alpha y - \alpha y \frac{x^2 + y^2}{R^2}] \\
\varepsilon \dot{z} &= z(2-z)[z + m(x^2 + y^2) - h] - \varepsilon c(z-1)
\end{aligned}
\tag{2.18}
$$

Figure 2.19 shows the resulting strange attractor

19
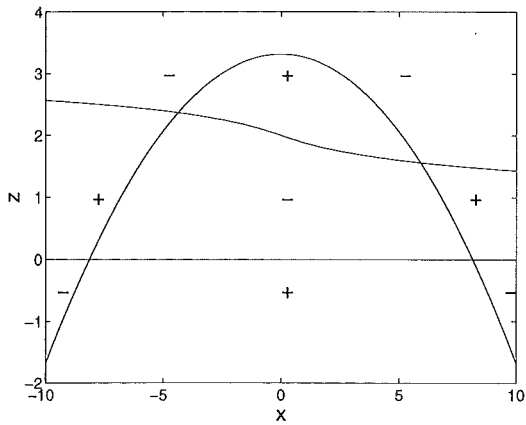
Figure 2.16: Cross-section of the perturbed toroid switch on the $xz$-plane, showing the nullclines of $z$ for $\varepsilon = 0$ + and − symbols indicate the sign of $\dot{z}$ in various regions.
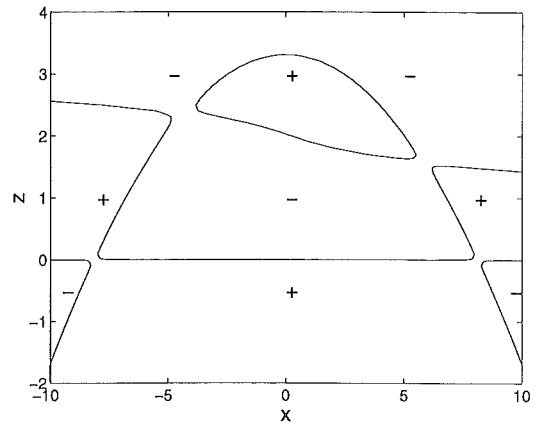
Figure 2.17: Cross-section of the perturbed toroid switch on the $xz$-plane, showing the nullclines for $\dot{z}$ for $\varepsilon > 0$ + and − symbols indicate the sign of $\dot{z}$ in various regions.
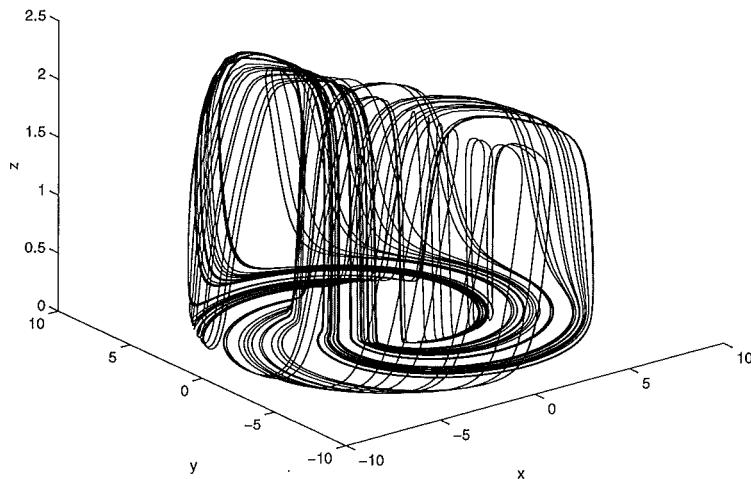


Figure 2.18: Folded toroid attractor from equations 2.17, with $a = 3, b = 0.8, c = 1, d = 0.1, m = 0.05, h = 3.312, R = 10, \lambda = -2, \mu = 1, \alpha = 2.8, \beta = 5$ and $\varepsilon = 0.1$
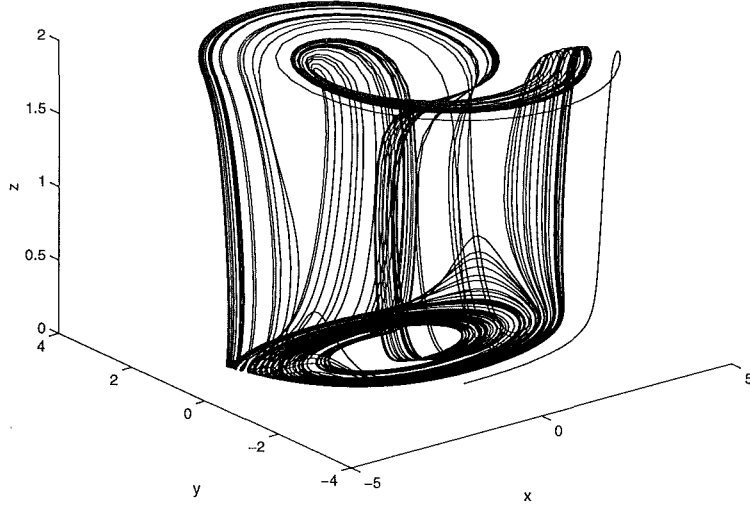
Figure 2.19: Elliptical toroid attractor from equations 2.18, with $a = 5, c = 1, m = 0.26, h = 2.76, R = 5, \lambda = -2, \mu = -10, \alpha = 1, \beta = 4$ and $\varepsilon = 0.03$

### 2.3.4 Combination Switches

#### ZZ-switch

We now put one Z-Switch on top of another to create a system with three branches to its slow subsystem. This ZZ-Switch has the form:

$$\varepsilon \dot{z} = z(2-z)(2+z)[z - 2a(x/3+1)][z - 2b(x/3-1)] - \varepsilon c(z+x) \qquad (2.19)$$

Figures 2.20 and 2.21 show the nullclines of $z$ for the ZZ-Switch with $\varepsilon = 0$ and $\varepsilon > 0$ respectively.

#### Dual Shil'nikov Orbit

The Shil'nikov orbit in equations 2.9 lay entirely on one side of the stable manifold of the central fixed point. With the ZZ-Switch, can extend this to a system in which the homoclinic orbit can lead from the unstable manifold of the fixed point to either side of the stable manifold. The equations

$$
\begin{aligned}
\dot{x} &= -z(z+2)(x-x_1) - z(z-2)(x-x_2) \\
&\quad + (4-z^2)[\alpha x - \beta y - \alpha x \frac{(x-2)^2 + y^2}{R^2}] \\
\dot{y} &= -z(z+2)(y-y_1) - z(z-2)(y-y_2) \\
&\quad + (4-z^2)[\beta x - \alpha y - \alpha y \frac{(x-2)^2 + y^2}{R^2}] \\
\varepsilon \dot{z} &= z(4-z^2)[z - 2a(x/3+1)][z - 2b(x/3-1)] - \varepsilon c(z+x)
\end{aligned}
\qquad (2.20)
$$

define such a system. A fixed point exists at the origin, with unstable manifold defined by the $xy$-dynamics on the $z = 0$ branch of the slow subsystem. Two turning edges exist on this branch, one of which turns trajectories to the upper $z = 2$ branch, while the other directs them to the lower $z = -2$ branch. On each of the outer branches trajectories are attracted towards

21
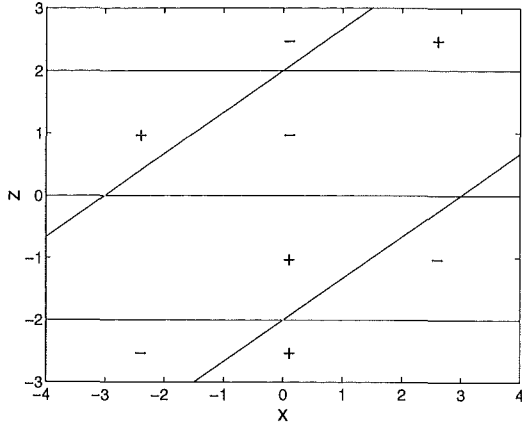
Figure 2.20: Nullclines of $z$ for the ZZ-switch with $\varepsilon = 0$ + and − symbols indicate the sign of $\dot{z}$ in various regions.
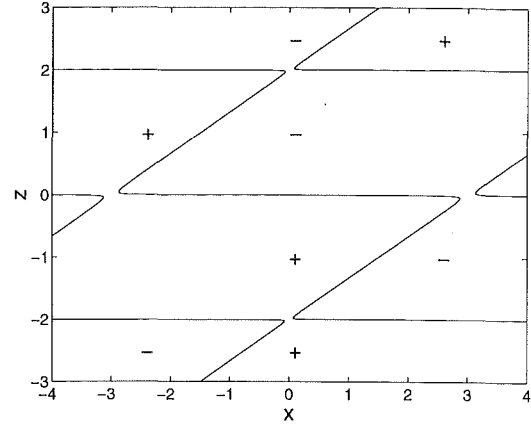
Figure 2.21: Nullclines of $z$ for the ZZ-switch with $\varepsilon > 0$ + and − symbols indicate the sign of $\dot{z}$ in various regions.

$x = 0$, $y = 0$, where a single turning edge sends them back towards the origin. Figure 2.22 shows the attractor generated by this system.

**Triple Spiral**

Using the ZZ-Switch, we here produce a system with three spiral oscillators, analogous to the double spiral system in section 2.3.1:

$$
\begin{aligned}
\dot{x} &= z(z+4)f_1 + (16-z^2)f_2 + z(z-4)f_3 \\
\dot{y} &= z(z+4)g_1 + (16-z^2)g_2 + z(z-4)g_3 \\
\varepsilon\dot{z} &= z(16-z^2)[z-a(x-c)][z-b(x+4)] - \varepsilon c(z+x)
\end{aligned}
\qquad (2.21)
$$

where

$$
\begin{aligned}
f_1 &= \phi(x,y,0.5,3,-4,0) \\
f_2 &= \phi(x,y,0.5,2,0,0) \\
f_3 &= \phi(x,y,0.5,3,4,0) \\
g_1 &= \psi(x,y,0.5,3,-4,0) \\
g_2 &= \psi(x,y,0.5,2,0,0) \\
g_3 &= \psi(x,y,0.5,3,4,0)
\end{aligned}
$$

and

$$
\begin{aligned}
\phi(x,y,\alpha,\beta,x_0,y_0) &= \alpha(x-x_0)-\beta(y-y_0) \\
&\quad - \alpha(x-x_0)\frac{(x-x_0)^2+(y-y_0)^2}{R^2} \\
\psi(x,y,\alpha,\beta,x_0,y_0) &= \beta(x-x_0)+\alpha(y-y_0) \\
&\quad - \alpha(x-x_0)\frac{(x-x_0)^2+(y-y_0)^2}{R^2}
\end{aligned}
$$

Figure 2.23 shows a triple spiral attractor.

22
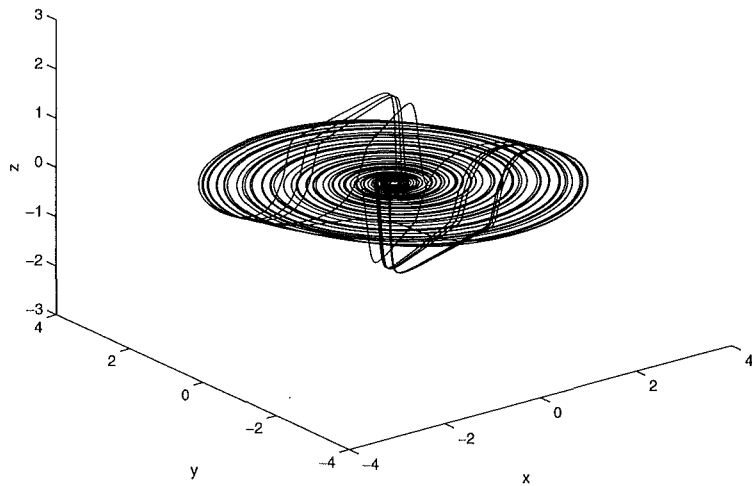
Figure 2.22: Two Shil'nikov orbits of the same equilibrium point, from equations 2.20, with $a = 1.15, b = 1.15, c = 1, R = 4\alpha = 0.5, \beta = 6, x_1 = -x_2 = 1.5, y_1 = -y_2 = 0.5$ and $\varepsilon = 0.1$
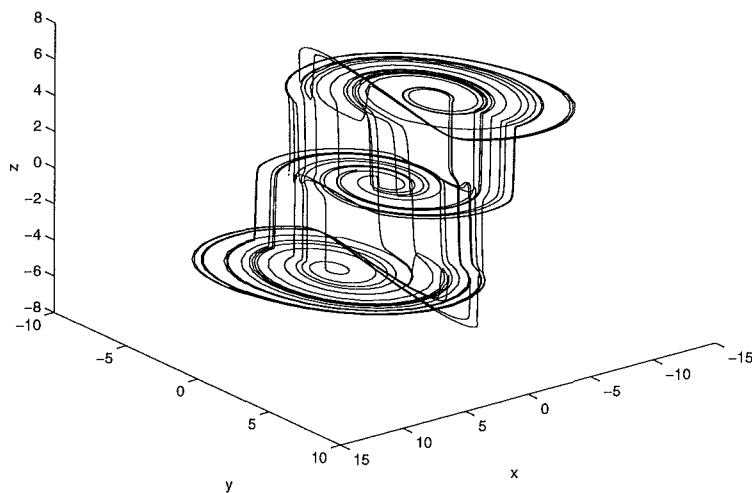


Figure 2.23: A triple spiral attractor from equations 2.21, with $a = b = 1, c = 4, \varepsilon = 0.09$ and $f_i, g_i$ defined as in text
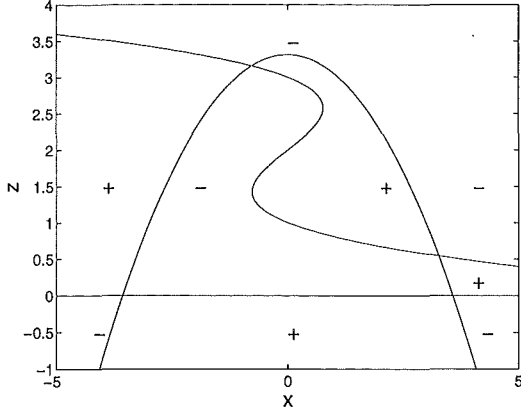
Figure 2.24: Nullclines of $z$ for the toroid-Z-switch with $\varepsilon = 0$ + and − symbols indicate the sign of $\dot{z}$ in various regions.
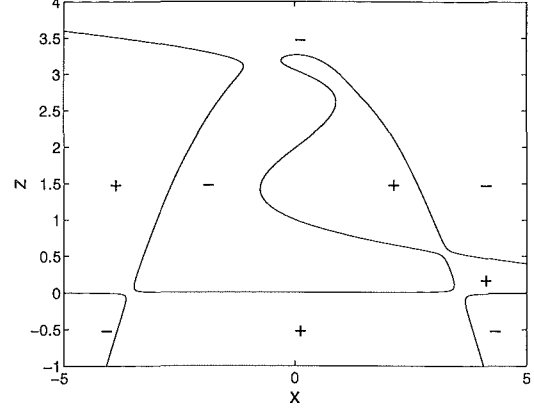
Figure 2.25: Nullclines of $z$ for the toroid-Z-switch with $\varepsilon > 0$ + and − symbols indicate the sign of $\dot{z}$ in various regions.

### Toroid-Z-switch

We now return to the folded toroid system described by equation 2.17 in section 2.3.3. If we take $b < 0$, the upper branch of the slow manifold folds into a Z-switch, as shown in figures 2.24 and 2.25, creating a combination Toroid-Z-Switch. Figures 2.26 and 2.27 show two further attractors for the folded toroid system.

### Toroid-toroid-switch

In the following example two toroid switches are placed side-by-side to create an invariant double toroid. The system is based on a fast subsystem defined by the equations

$$\varepsilon \dot{z} = z(1.5 - z)[z - 1 + H(x,y)] + \varepsilon(3/4 - z) \tag{2.22}$$

where

$$H(x,y) = \frac{(x-y)^4}{64} - \frac{x^2 - y^2}{2} + \frac{(x+y)^2}{4} \tag{2.23}$$

Figures 2.28 and 2.29 show cross sections of the toroid-toroid-switch in the $xz$-plane for $\varepsilon = 0$ and $\varepsilon > 0$. Turning edges occur at $1 - H(x,y) = 0$ and $1 - H(x,y) = 1.5$, as shown figure 2.30.

### Invariant Double Toroid

This system is analogous to the system described in section 2.3.3. The equations

$$
\begin{aligned}
\dot{x} &= a(1.5 - z)x(x^2 - 8)/16 \\
&\quad + bz[\alpha(\alpha x + \beta y)[8 - (\alpha x + \beta y)^2]/16 - \beta(\beta x - \alpha y)] \\
\dot{y} &= a(1.5 - z)y \\
&\quad + bz[\beta(\alpha x + \beta y)[8 - (\alpha x + \beta y)^2]/16 + \alpha(\beta x - \alpha y)] \\
\varepsilon \dot{z} &= z(1.5 - z)[z - 1 + H(x,y)] + \varepsilon(3/4 - z) \tag{2.24}
\end{aligned}
$$

where

$$\alpha = \cos(\theta)$$

24
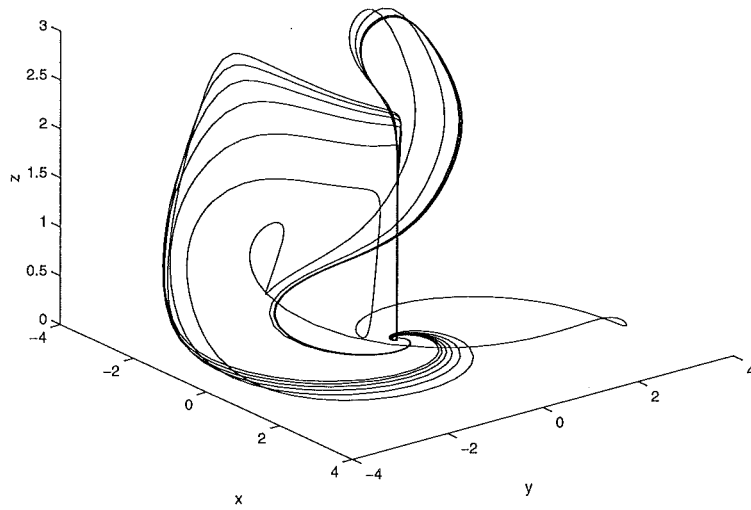
Figure 2.26: Folded toroid attractor from equations 2.17, with $a = 2, b = -0.08, c = 1, d = 1, m = 0.26, h = 2.76, R = 5, \lambda = -2, \mu = 1, \alpha = 3, \beta = -4$ and $\varepsilon = 0.5$
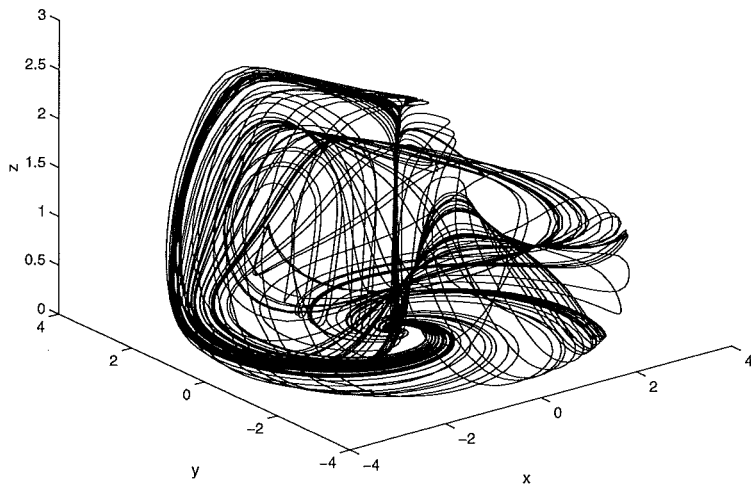


Figure 2.27: Folded toroid attractor from equations 2.17, with $a = 3, b = 0.3, c = 1, d = 1, m = 0.26, h = 2.76, R = 5, \lambda = -2, \mu = 1, \alpha = 3, \beta = -5$ and $\varepsilon = 0.5$
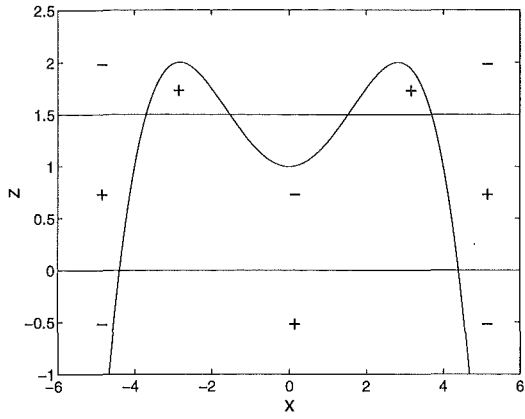
Figure 2.28: Nullclines of $z$ for the toroid-toroid-switch with $\varepsilon = 0$ + and − symbols indicate the sign of $\dot{z}$ in various regions.
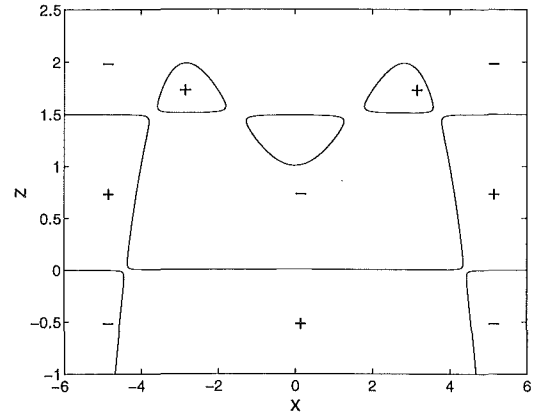
Figure 2.29: Nullclines of $z$ for the toroid-toroid-switch with $\varepsilon > 0$ + and − symbols indicate the sign of $\dot{z}$ in various regions.
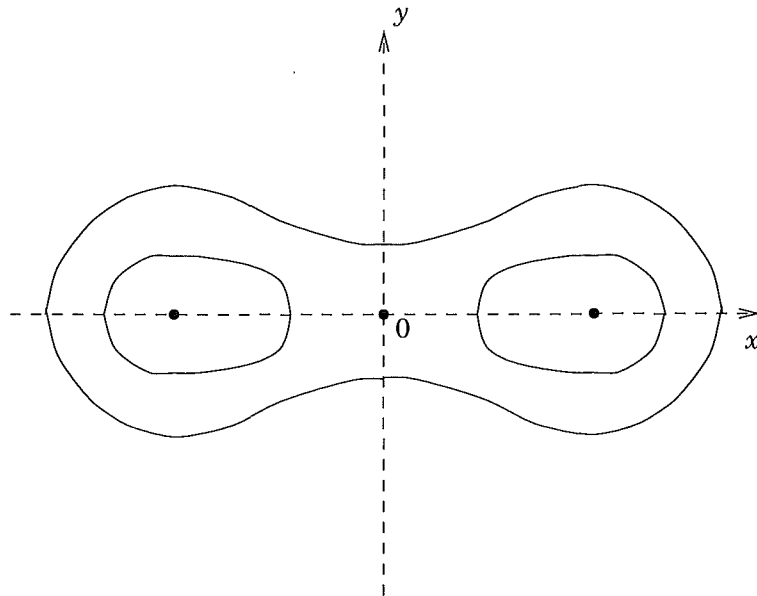


Figure 2.30: Turning edges of the Toroid-Z switch subsystem for $\varepsilon = 0$
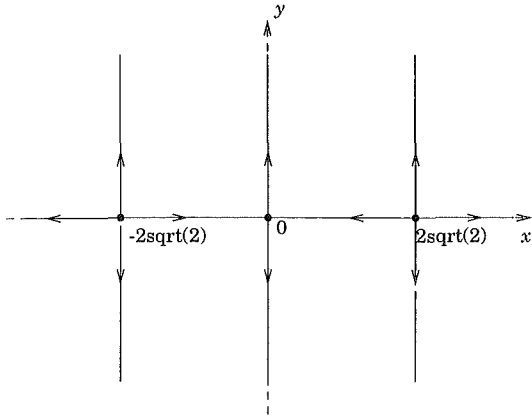
Figure 2.31: Phase portrait for the reduced slow subsystem (2.26) on the $z = 0$ branch.
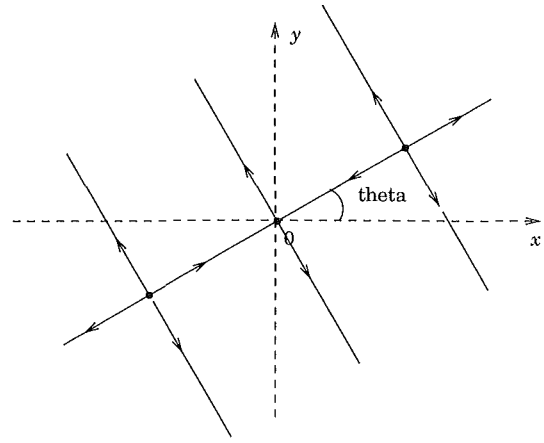


Figure 2.32: Phase portrait for the reduced slow subsystem on the $z = 1.5$ branch.

$$\beta = \sin(\theta)$$

$$H = (x-y)^4/64 - (x^2-y^2)/2 + (x+y)^2/4 \qquad (2.25)$$

reduce to

$$\dot{x} = 1.5ax(x^2-8)/16$$

$$\dot{y} = 1.5ay \qquad (2.26)$$

on the lower branch $z = 0$. This reduced system has a saddle point at the origin and two repelling fixed points at $(\pm 2\sqrt{2}, 0)$, as shown in figure 2.31. The upper $z = 1.5$ branch is similar, but time-reversed and rotated by $\theta$ degrees about the origin.

Figure 2.33 shows several trajectories generated from the invariant double toroid system. More than one trajectory was required to describe the system, as it has two attracting and two repelling periodic orbits. The attracting orbits are visible as dense regions in figure 2.33, and the repelling orbits as gaps (the trajectories begin near these repelling orbits).

### Perturbed Double Toroid

As for the invariant single toroid system in section 2.3.3, the invariant double toroid system can be made chaotic by minor modifications. The following system is an example of a perturbed double toroid system:

$$\dot{x} = a(1.5-z)(-\frac{\partial H}{\partial y}) + bz[\alpha(\alpha x + \beta y)$$
$$\times [8 - (\alpha x + \beta y)^2]/16 - \beta(\beta x - \alpha y)]$$
$$\dot{y} = a(1.5-z)(-\frac{\partial H}{\partial y} + cy) + bz[\beta(\alpha x + \beta y) \qquad (2.27)$$
$$\times [8 - (\alpha x + \beta y)^2]/16 + \alpha(\beta x - \alpha y)]$$
$$\varepsilon\dot{z} = z(1.5-z)[z-1+H(x,y)] + \varepsilon(3/4-z)$$

### 2.3.5 Systems with Delta-Switches

#### The Delta-Switch

Figures 2.34 and 2.35 show a 'delta-switch' for $\varepsilon > 0$, with equation

27
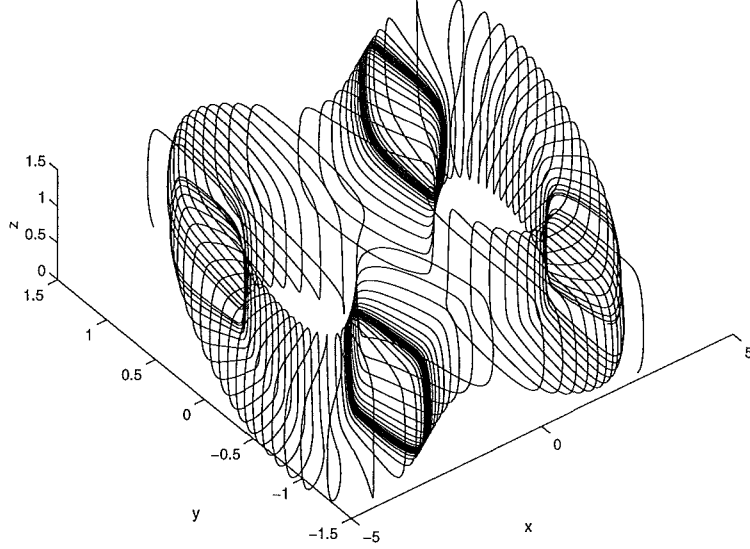
Figure 2.33: Invariant double toroid attractor from equations 2.24, with $a = b = 1$, $\theta = 0.08$ and $\varepsilon = 0.06$

$$\varepsilon \dot{z} = (z+1)(z-1)(z-x-1)(z+x-1) - \varepsilon z \qquad (2.28)$$

It is a slight modification of the Z-switch, with a second diagonal nullcline of $z$ intersecting the first on the upper branch of the slow subsystem.

**A system that switches between two states of the upper branch**

This system uses the delta-switch to exhibit a chaotic switching between two states on the upper branch of the slow subsystem.

$$
\begin{aligned}
\dot{x} &= (z+1)(-x) - (z-1)(ax+y) \\
\dot{y} &= (z+1)(-y) - (z-1)(ay-x) \\
\varepsilon \dot{z} &= (z+1)(z-1)(z-x-1)(z+x-1) - \varepsilon z
\end{aligned}
\qquad (2.29)
$$

The switching mechanism is on the lower branch, selecting one of two states (left, right) on the upper branch, as shown in figure 2.36. Trajectories spiral out from a saddle point at $(-1, 0, 0)$, until they hit one of the two turning points at $x = \pm 2$, where they are switched to the upper branch. For a sufficiently tight spiral, which turning point a trajectory eventually hits is dependent on the point at which the trajectory arrives on the lower branch. In this example, the upper branch has a single attracting fixed point at $(1, 0, 0)$. The chaotic behaviour of the system can also be affected by modifying the strength of this fixed point.

**A system that switches between two lobes on the upper branch**

This system is similar to the previous, with the upper branch modified so that a figure-eight closed orbit replaces the single fixed point. As before, the flow on the lower branch leads a

28
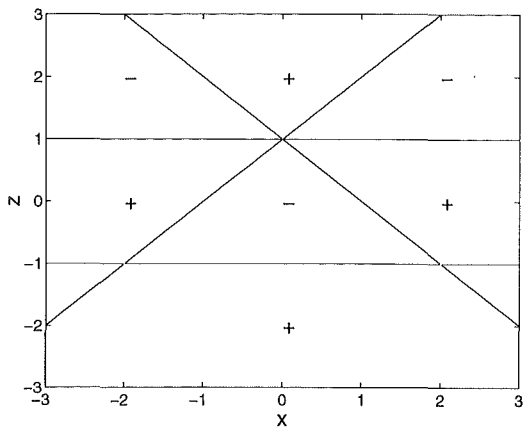
Figure 2.34: Nullclines of $z$ for the $\Delta$-switch with $\varepsilon = 0 +$ and $-$ symbols indicate the sign of $\dot{z}$ in various regions.
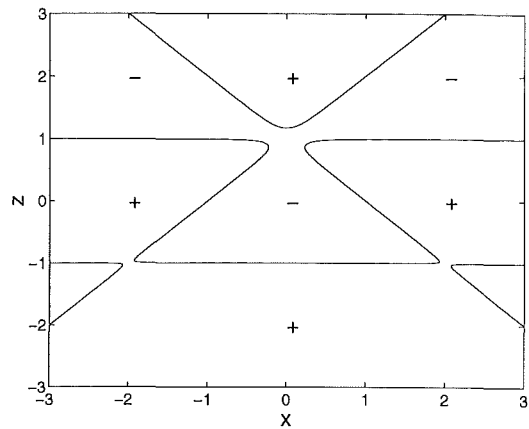
Figure 2.35: Nullclines of $z$ for the $\Delta$-switch with $\varepsilon > 0 +$ and $-$ symbols indicate the sign of $\dot{z}$ in various regions.
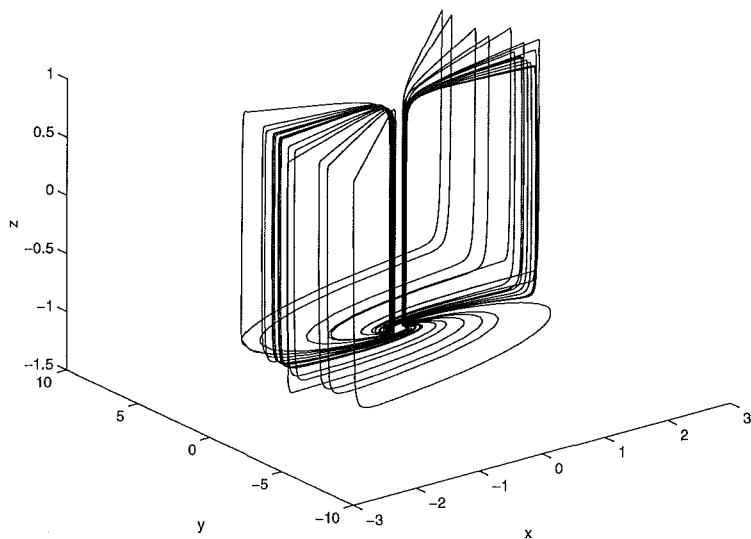


Figure 2.36: Two state attractor from equations 2.29, with $a = 0.9$

29
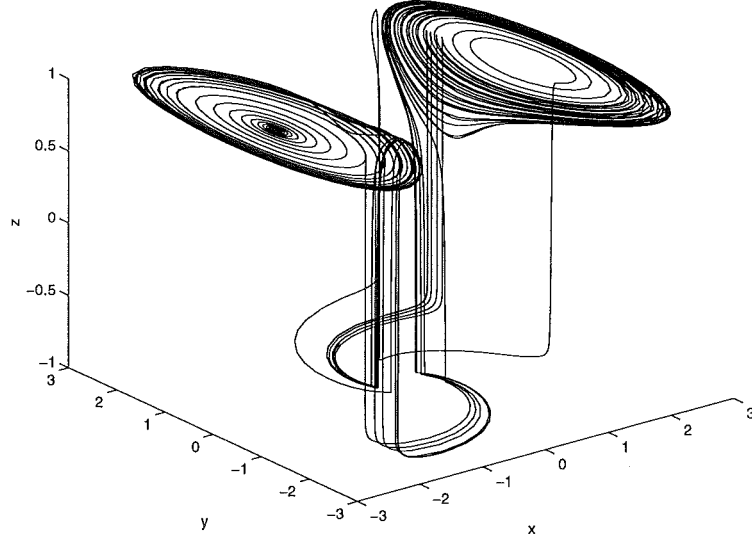
Figure 2.37: Figure 8 two state attractor from equations 2.30, with $a = 0.3$, $b = 5$, $R = 2.9$, $d = 0.85$ and $c = 100$

trajectory to one of the two turning points, from which it is directed to one of the two lobes of the figure-eight.

$$
\begin{aligned}
\dot{x} &= (z+1)f_x - (z-1)g_x \\
\dot{y} &= (z+1)f_y - (z-1)g_y \\
\varepsilon\dot{z} &= c((z+1)(z-1)(z-x-1)(z+x-1) - \varepsilon z)
\end{aligned}
\tag{2.30}
$$

where

$$
\begin{aligned}
f_x &= 4(a(x-2)(x+2)x - by - \frac{a(x-2)(x+2)x(x^2+y^2)}{R^2}) \\
f_y &= 4(b(x-2)(x+2)x + ay - \frac{ay(x^2+y^2)}{R^2}) \\
g_x &= dx + y \\
g_y &= -x + dy
\end{aligned}
\tag{2.31}
$$

This system is shown in figure 2.37. Although the figure is apparently similar to the Lorenz attractor, the switching mechanism and the arrangement of $z$-nullclines are different.

## 2.4 Timing constants

In equations 2.30 the equation for the fast subsystem was multiplied by a constant $c$, with a value of 100 for the attractor shown in figure 2.37. This constant adjusts the relative strengths of fast and slow subsystems, in this case increasing the strength of the fast subsystem a hundredfold.

Figure 2.38 shows the same system, with a lower value for $c$. Trajectories on the upper branch remain on the upper branch indefinitely, because when they pass near the turning point at $x = 0$ the fast subsystem is not strong enough to pull them to the lower branch before they move back away from the turning point. Figure 2.39 shows the system with a
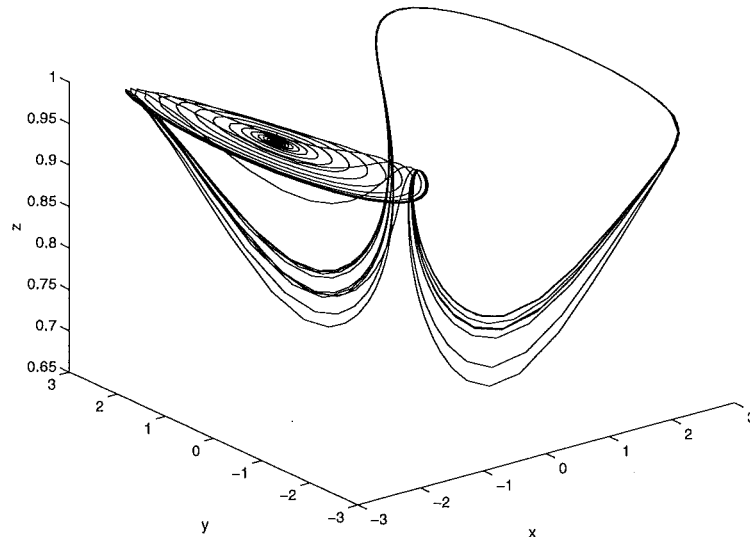
Figure 2.38: Figure 8 two state attractor from equations 2.30, with $c$ too small

higher value for $c$. Trajectories oscillate repeatedly between the upper and lower branches, because the fast subsystem is strong enough to pull them back before the slow subsystem can significantly affect their motion. Similar situations can be observed in many other systems.

The constant $c$ can be considered to be a ratio of the time trajectories on the system take to travel a given distance in the direction of the fast subsystem to the time trajectories take to travel the same distance on a branch of the slow subsystem.

We can approximate each subsystem by a linear system $\dot{x} = \lambda x$, where $\lambda$ is the dominant eigenvalue of the linearized flow around a fixed point with eigenvector pointing in the direction of the subsystem. This gives an estimate of the time spent on the subsystem. This approximation will be reasonably accurate for the fast subsystem, on which the motion of the trajectories is nearly linear. It will be less so for the slow subsystem, but the approximation will give an order of magnitude of $c$.

The value of $c$ can then be refined by experimental means. For this thesis graphical output from MATLAB was used to select a value for $c$ that gave the system the desired qualitative behaviour.
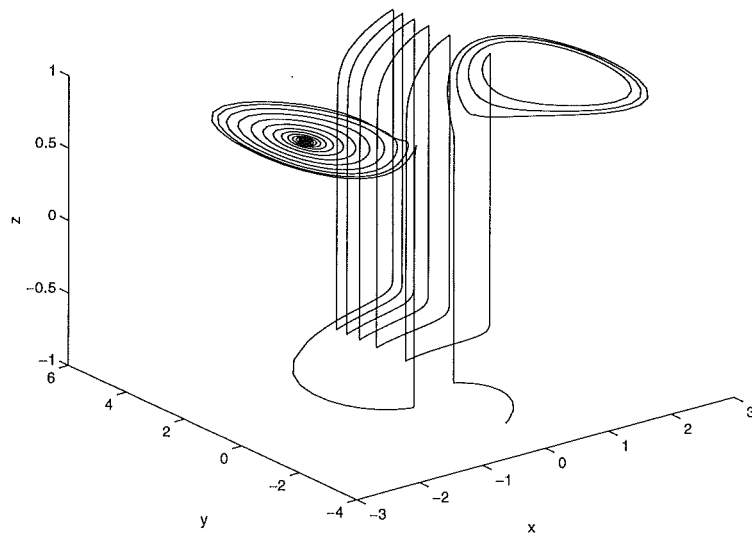
Figure 2.39: Figure 8 two state attractor from equations 2.30, with $c$ too large

# Chapter 3

# The Lorenz Equations

## 3.1 Lorenz Equations

### 3.1.1 History

The Lorenz equations have played a prominent role in the development of nonlinear dynamics. They were developed by the meteorologist Lorenz as a simplification of the Navier-Stokes equations describing fluid convection. Three variables, $x$, $y$ and $z$ represent convective overturn and horizontal and vertical temperature variation respectively. Parameters $\sigma$ and $\rho$ are proportional to the Prandtl and Rayleigh numbers. Investigation of the equations by Lorenz revealed the famous 'butterfly attractor', and stimulated further investigations into the behaviour of nonlinear systems.

Although they do not constitute a realistic model of weather for values of $\rho \gg 1$, where the interesting chaotic behaviour occurs, the Lorenz Equations have since been found to usefully model other physical systems, including convection in a toroidal region, disc dynamos, and spiking phenomena in lasers.

For the purposes of this thesis, I will first consider behaviour of system at $\rho = 28$ (with the other two parameters fixed at $\sigma = 10$ and $\beta = 8/3$), at which the Lorenz Attractor is observed and later explore properties of system at other values of $\rho$.

### 3.1.2 Equations

The Lorenz System is defined by the equations

$$\dot{x} = \sigma(y - x)$$
$$\dot{y} = \rho x - y - xz$$
$$\dot{z} = -\beta z + xy$$

where the parameters $\sigma, \rho, \beta > 0$. The system is invariant under the transformation $(x, y, z) \rightarrow (-x, -y, z)$.

At $\rho = 28$, the system has three fixed points: one at the origin, and two others:

$$P^+ = (\sqrt{\beta(\rho - 1)}, \sqrt{\beta(\rho - 1)}, \rho - 1)$$
$$P^- = (-\sqrt{\beta(\rho - 1)}, -\sqrt{\beta(\rho - 1)}, \rho - 1)$$
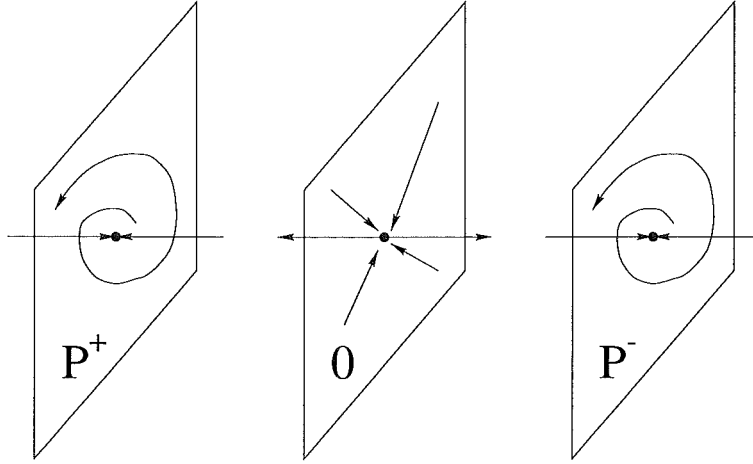
Figure 3.1: A diagram of the fixed points of the Lorenz system for $\rho = 28$

The linearized flow near the origin has eigenvalues

$$\lambda_{1,2} = \frac{-\sigma - 1 \pm \sqrt{(\sigma - 1)^2 + 4\rho\sigma}}{2}$$

$$\lambda_3 = -\beta \tag{3.1}$$

which, for $\sigma = 10$, $\beta = 8/3$ and $\rho = 28$ makes it a saddle, with two-dimensional stable manifold and one-dimensional unstable manifold.

The linearized flows near $P^+$ and $P^-$ have eigenvalues given by the roots of

$$\lambda^3 + (\sigma + \beta + 1)\lambda^2 + \beta(\sigma + \rho)\lambda + 2\sigma\beta(\rho - 1) = 0 \tag{3.2}$$

For $\sigma = 10, \beta = 8/3$ and $\rho = 28$, one eigenvalue is real and negative and the other two are complex conjugates with positive real parts. Thus these fixed points each have a one-dimensional stable manifold and a two-dimensional unstable manifold. Figure 3.1 is a diagrammatic view of these fixed points. Figures 3.2 and 3.3 show the strange attractor traced by trajectories of this system.

## 3.2 A Pseudo-Lorenz Attractor

This system reproduces the qualitative features of the Lorenz attractor for $\rho = 28$, preserving the number and nature of fixed points. Under the scheme described by Deng, the sections of the slow subsystem were attracting surfaces. Attracting surfaces are generally easier to find than invariant surfaces. However, this limits the range of possible fixed points. In the case of the Lorenz attractor, we wish the fixed points $P^+$ and $P^-$ to have two-dimensional unstable manifolds and one-dimensional stable manifolds. In Deng's scheme, this would correspond to a two-dimensional slow subsystem and one-dimensional fast subsystem, with $P^+$ and $P^-$ lying on two branches of the slow subsystem. However, the basins of attraction of these two fixed points are divided by the non-attracting stable manifold of the fixed point at the origin. Deng's scheme would require that any branch of the slow subsystem corresponding to this manifold be attracting.

We can bypass this requirement, and describe the dynamics on a non-attracting plane, by specifying sections in the slow subsystem that do not correspond to nullclines of the fast

34
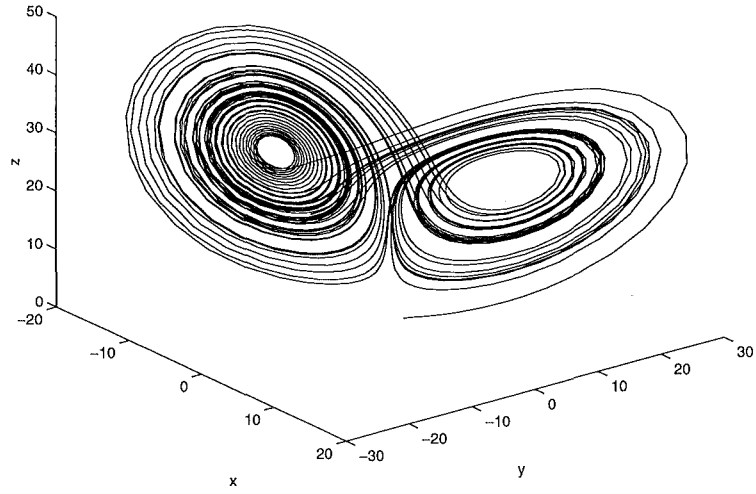
Figure 3.2: The Lorenz Attractor from equations 3.1, with $\sigma = 10$, $\beta = 8/3$ and $\rho = 28$
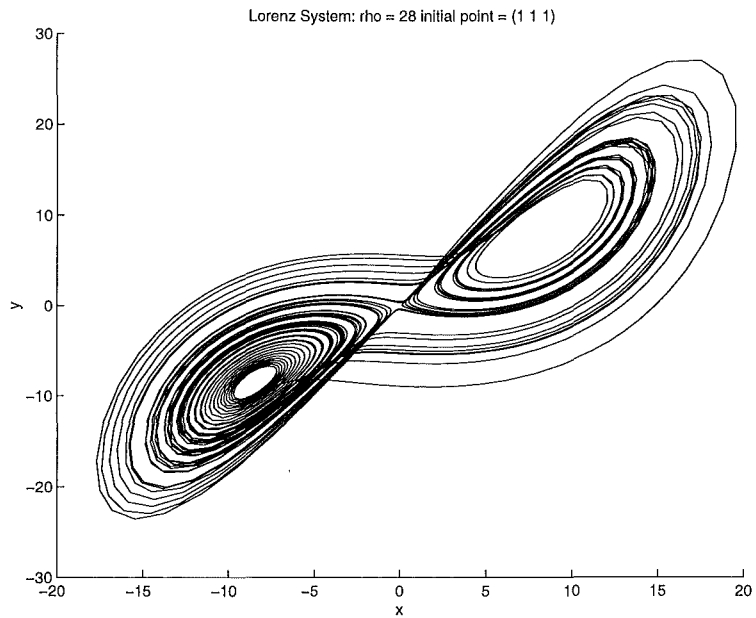


Figure 3.3: The Lorenz Attractor from equations 3.1, with $\sigma = 10$, $\beta = 8/3$ and $\rho = 28$

subsystem. In this case, we use a standard Z-switch, but add a third branch to the slow subsystem between the previous two, at $z = 0$. We can describe the $xy$-dynamics on this third branch independently of the $z$-dynamics of the fast subsystem.

The system

$$\dot{x} = (z+2)zf_x + (z+2)(2-z)g_x - (2-z)zh_x$$
$$\dot{y} = (z+2)zf_y + (z+2)(2-z)g_y - (2-z)zh_y$$
$$\varepsilon\dot{z} = 0.1(2+z)(2-z)(z-mx) - \varepsilon cz \qquad (3.3)$$

where

$$f_x = 0.1x - y$$
$$f_y = 0.1y + x$$
$$g_x = -x$$
$$g_y = -y$$
$$h_x = 0.1x - y$$
$$h_y = 0.1y + x \qquad (3.4)$$

reproduces the qualitative behaviour of the Lorenz Attractor for $\rho = 28$. On the upper ($z = 2$) and lower ($z = -2$) branches, trajectories spiral outwards from fixed points corresponding to $P^+$ and $P^-$, until they reach the turning points of the Z-switch, and switch branches.

On the $z = 0$ branch, equations 3.3 and 3.4 reduce to:

$$\dot{x} = -4x$$
$$\dot{y} = -4y$$
$$\dot{z} = -\frac{0.4}{\varepsilon}mx \qquad (3.5)$$

so that trajectories are pulled towards zero in the $x$- and $y$-directions, while still moving in the $z$-direction between the attracting upper and lower branches. When they arrive at one or other outer branch, they have been pulled towards the centre of the spiral on that branch.

The stability of the attractor is sensitive to the relative strengths of the fast and slow subsystems. If the eigenvalues describing the fast subsystem are too much larger than those describing the slow subsystem, trajectories will not be sufficiently attracted towards the origin, and will not return to the centre of the opposite spiral. Over several passes, the spiral will continue to grow until it passes out of the stable region of the Z-switch, and the trajectory will not return. In order to prevent this happening, a timing constant is inserted to reduce the strength of the fast subsystem with respect to the slow. Figure 3.4 shows the strange attractor produced by this system.

The visual similarity to the Lorenz Attractor can be enhanced by swapping $x$ and $z$ in equations 3.3, making the fast subsystem act in the $x$-direction, switching between branches parallel to the $yz$-plane. The Z-switch becomes an N-switch, and the attractor generated is shown in figure 3.5.
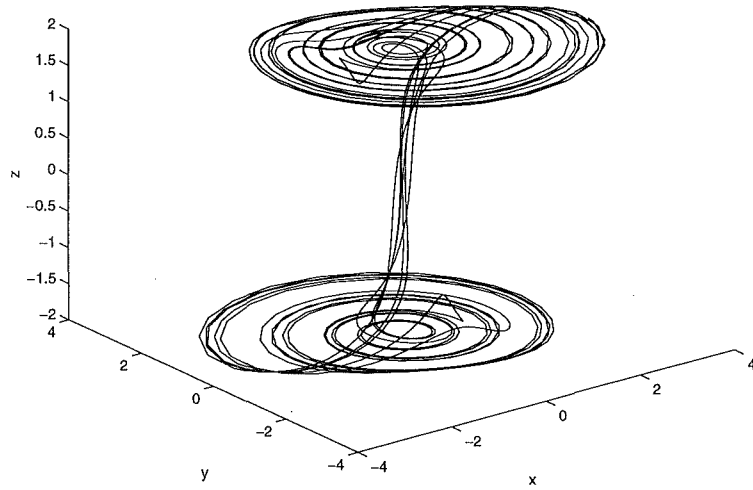
Figure 3.4: Pseudo-Lorenz attractor from equations 3.3, with $m = 1.543$, $\varepsilon = 0.1$ and $c = 1$
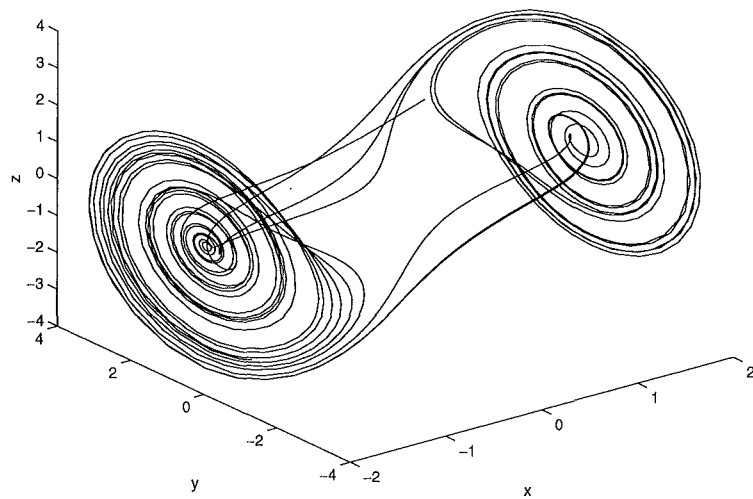


Figure 3.5: Pseudo-Lorenz Attractor with the fast subsystem acting in the $x$-direction

| $\rho$ | Eigenvalues at origin | Eigenvalues at $P^+$ and $P^-$ |
|---|---|---|
| $\rho < 1$ | all real and negative | |
| $\rho = 1$ | one zero, two negative | one zero, two negative |
| $1 < \rho < \rho_s \approx 1.346$ | one positive, two negative | three real, negative |
| $\rho = \rho_s$ | one positive, two negative | three negative (two equal) |
| $\rho_s < \rho < \rho_H \approx 24.74$ | one positive, two negative | one negative real, two negative complex conjugates |
| $\rho_H < \rho$ | one positive, two negative | one negative real, two positive complex conjugates |

Table 3.1: Eigenvalues of the linearized flows around fixed points in the Lorenz equations, for different values of $\rho$

## 3.3 Bifurcation

### 3.3.1 Bifurcation properties of the Lorenz Attractor

The behaviour of a system over a range of parameter values is often studied. Commonly, the number and types of fixed points and other features of a system will vary depending on the values of parameters. The behaviour of the Lorenz attractor varies with different values of $\rho$.

For all values of $\rho$ there is a fixed point at the origin. For $\rho < 1$, this is a hyperbolic attractor, and the only fixed point of the system.

At $\rho = 1$, a "pitchfork" bifurcation occurs. The fixed point at the origin becomes a saddle, with a two-dimensional unstable manifold and one-dimensional stable manifold. Simultaneously, two other fixed points, $P^+$ and $P^-$ appear. These fixed points initially have all eigenvalues real and negative. Thus the unstable manifold of the origin leads from the saddle directly to the attracting fixed points $P^+$ and $P^-$. The stable manifold of the saddle divides the two basins of attraction.

As $\rho$ increases further, two of the eigenvalues of the fixed points $P^+$ and $P^-$ converge and become equal at $\rho = \rho_s \approx 1.346$. Thereafter, they become complex conjugates with negative real parts, and the unstable manifold of the origin begins to spiral into $P^+$ and $P^-$. This spiralling becomes more pronounced as $\rho$ increases. The magnitude of the negative real part of the complex eigenvalues reduces, while the magnitude of the imaginary part increases. At $\rho = \rho_H \approx 24.74$ the real parts pass through zero, and $P^+$ and $P^-$ lose stability in a Hopf bifurcation. Beyond $\rho_H$ the trajectory spirals outwards from $P^+$ and $P^-$, and the familiar butterfly attractor is formed.

Table 3.1 summarizes the properties of the eigenvalues of the three fixed points for different values of $\rho$.

### 3.3.2 A model attractor exhibiting similar properties

Equation 3.3 describes a system that reproduces qualitative features of the Lorenz system for $\rho = 28$, but does not mimic the bifurcation properties of that system. The model can be extended to include these bifurcations. The pitchfork bifurcation at $\rho = 1$ will be incorporated into a modified fast subsystem, and the Hopf bifurcation at $\rho = \rho_H$ into the slow subsystem.
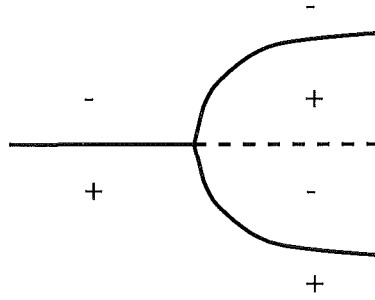
Figure 3.6: Pitchfork bifurcation

## Pitchfork bifurcation

The equation

$$\dot{x} = \mu x - x^3 \tag{3.6}$$

describes a generic one-dimensional pitchfork bifurcation. A fixed point exists at $x = 0$ for all values of $\mu$, which is stable for $\mu < 0$ and unstable for $\mu > 0$. For $\mu > 0$ there are two other stationary points, at $x = \pm\sqrt{\mu}$, both of which are stable. Figure 3.6 shows this bifurcation schematically.

This one-dimensional system will form the basis for a new two-dimensional 'pitchfork switch', in which nullclines of $x$ will correspond to the fixed points of equation 3.6. For the Lorenz Attractor, the pitchfork bifurcation occurs at $\rho = 1$, and the two fixed points created in the bifurcation ($P^+$ and $P^-$) have positions $x = \pm\sqrt{\beta(\rho - 1)}$.

For the purposes of Deng's scheme, we cannot simply insert equation 3.6 into the fast subsystem, because the fast subsystem describes only attracting nullclines. Instead we must separate the fixed points with negative eigenvalues in the direction of the fast subsystem from those with positive eigenvalues. The former will be described by the fast subsystem, and the latter by sections in the slow subsystem.

The equation

$$\varepsilon\dot{x} = (x^2 - x_f^2)(\frac{\rho}{28}z - x) - \varepsilon x \tag{3.7}$$

where

$$x_f = \sqrt{\beta(\rho - 1)} \tag{3.8}$$

will serve as a fast subsystem for a pseudo-Lorenz model that switches in the $x$-direction, as in figure 3.5. Figures 3.7 and 3.8 show the nullclines of $x$ for this 'pitchfork switch' for $\rho < 1$ and $\rho > 1$. Note that for $\rho > 1$ we have a Z-Switch, as in section 3.2 for $\rho = 28$. For $\rho < 1$, the quadratic $x^2 - x_f^2$ has no real roots, and the only nullcline of $x$ is given by $\frac{\rho}{28}z - x = 0$. In conjunction with a non-attracting section such as the one in the system described by equations 3.3, this will reproduce the pitchfork bifurcation at $\rho = 1$.

## Hopf bifurcation

The equations

$$
\begin{aligned}
\dot{z} &= \mu z - \omega y \\
\dot{y} &= z + \mu y
\end{aligned}
\tag{3.9}
$$

39
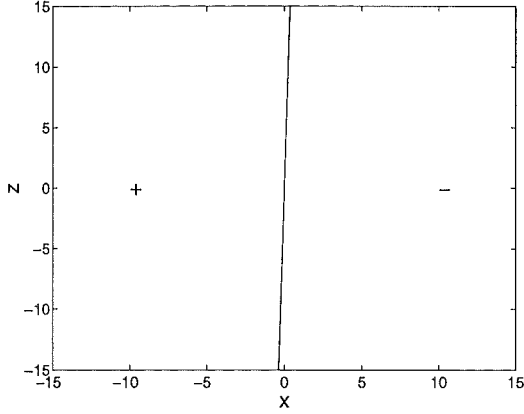
Figure 3.7: Nullclines of $x$ for the pitchfork-switch with $\rho < 1 +$ and $-$ symbols indicate the sign of $\dot{x}$ in various regions.
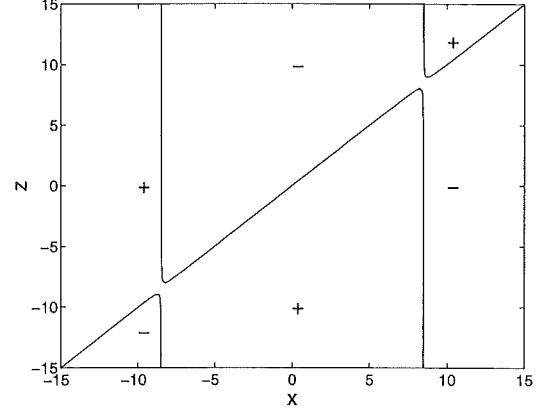
Figure 3.8: Nullclines of $x$ for the pitchfork-switch with $\rho > 1 +$ and $-$ symbols indicate the sign of $\dot{x}$ in various regions.

describe a Hopf bifurcation, with a single fixed point at the origin. The linearized vector field around this fixed point has eigenvalues $\lambda = \mu \pm \sqrt{-\omega}$. For $\omega > 0$, these eigenvalues are complex conjugates.

A Hopf bifurcation occurs when $\omega$ is positive, and the parameter $\mu$ changes sign. For $\mu < 0$ the fixed point is stable, so that trajectories spiral in towards it. For $\mu > 0$, the fixed point is unstable, and trajectories spiral outwards. At $\mu = 0$, the eigenvalues have zero real parts, and trajectories trace periodic orbits around the fixed point.

In the Lorenz attractor, the Hopf bifurcation takes place at $\rho = \rho_H = \sigma(\sigma + \beta + 3)/(\sigma - \beta - 1) \approx 24.74$. Thus, we can replace $\mu$ with $\rho - \rho_H$, in equation 3.9, and use it to describe the dynamics of the system on each of the branches of the slow subsystem, where Hopf bifurcations occur at the fixed points $P^+$ and $P^-$.

Another change in the Lorenz system occurs at $\rho_s \approx 1.346$. For $\rho < \rho_s$, the stable eigenvalues of $P^+$ and $P^-$ are entirely real. We can model this by replacing the parameter $\omega$ by a function that returns a positive value (as above) for $\rho > \rho_s$, but a negative value for $\rho < \rho_s$. The substitution $\omega = (\rho - \rho_s)$ will give the desired sign at all values of $\rho$.

Thus, we can include both the Hopf bifurcation at $\rho = \rho_H$ and the change from real to complex eigenvalues at $\rho = \rho_s$ by introducing the following equations for the flows on the branches of the slow manifold:

$$
\begin{aligned}
f_z &= (\rho - \rho_H)z - (\rho - \rho_s)y \\
f_y &= z + (\rho - \rho_H)y
\end{aligned}
\tag{3.10}
$$

Note that critical values $\rho_H$ and $\rho_s$ are specified explicitly in these equations, whereas they do not appear in the original Lorenz equations. Their values could be modified at will, without affecting other qualitative features of the system. This property is useful in modelling applications, where a system must be developed to match given data.

**A Pseudo-Lorenz system with similar bifurcation properties**

Full equations for the bifurcation model of the Lorenz attractor are as follows:
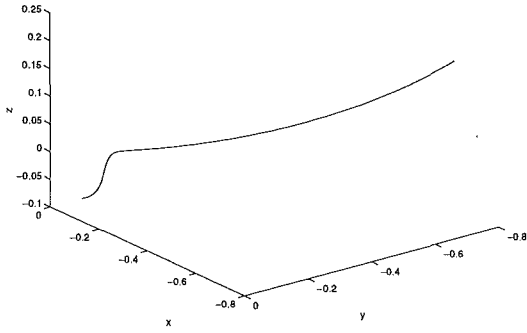
Figure 3.9: Lorenz attractor from equations 3.1, with $\rho = 1.2$, $\sigma = 10$ and $\beta = 8/3$. The trajectory runs from initial point $(0, -0.1, -0.1)$ to the fixed point $P^+$.
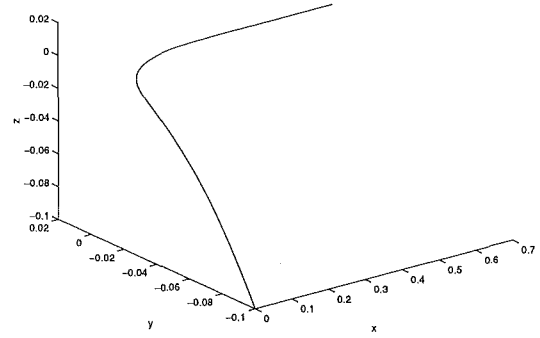
Figure 3.10: Bifurcating pseudo-Lorenz attractor from equations 3.11, with $\rho = 1.2$, $\sigma = 10$ and $\beta = 8/3$. The trajectory runs from initial point $(0, -0.1, -0.1)$ to the fixed point $P^+$.

$$\varepsilon \dot{x} = \frac{0.6}{\rho}((x^2 - x_f^2)(\frac{\rho}{28}z - x) - \varepsilon x)$$

$$\dot{y} = (x + x_f)xf_y + (x + x_f)(x_f - x)g_y - (x_f - x)xf_y$$

$$\dot{z} = (x + x_f)xf_z + (x + x_f)(x_f - x)g_z - (x_f - x)xf_z \qquad (3.11)$$

where

$$x_f = \sqrt{\beta(\rho - 1)} \qquad (3.12)$$

and

$$f_z = \frac{A(\rho - \rho_H)z - B(\rho - \rho_s)y}{2x_f^2}$$

$$f_y = \frac{Bz + A(\rho - \rho_H)y}{2x_f^2}$$

$$g_z = \frac{-z}{\rho - 1}$$

$$g_y = \frac{-\rho y}{\beta(\rho - 1)}$$

$$A = \frac{5}{\rho}$$

$$B = 2 \qquad (3.13)$$

Figures 3.10, 3.12, 3.14 and 3.16 illustrate the behaviour of the system described by equations 3.11 at different values of $\rho$, in comparison for the behaviour of the Lorenz system at the same $\rho$ values, shown in figures 3.9, 3.11, 3.13 and 3.15. Note that the scale and direction of the axes are not the same in corresponding figures: they have been adjusted to make comparison of the behaviour of the two systems easier.
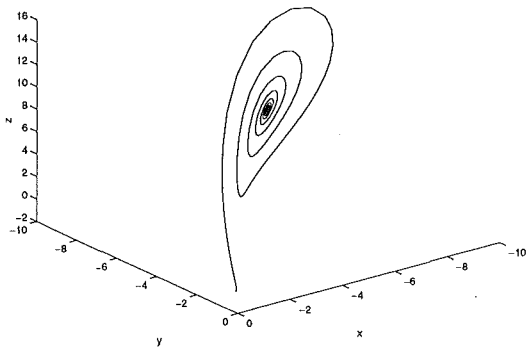
Figure 3.11: Lorenz attractor from equations 3.1, with $\rho = 10$, $\sigma = 10$ and $\beta = 8/3$
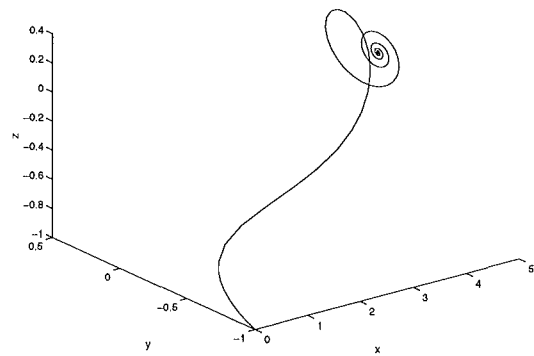


Figure 3.12: Bifurcating pseudo-Lorenz attractor from equations 3.11, with $\rho = 10$, $\sigma = 10$ and $\beta = 8/3$. The parameter $B$ was raised to 20 for this plot, to enhance the spiralling motion near the fixed point $P^+$. Spiralling is also evident, but less pronounced, at $\rho = 10$ for lower values of $B$.
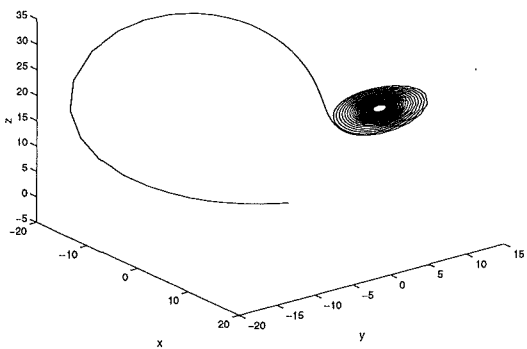


Figure 3.13: Lorenz attractor from equations 3.1, with $\rho = 20$, $\sigma = 10$ and $\beta = 8/3$
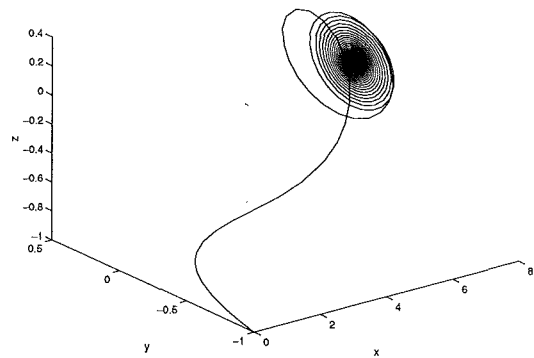


Figure 3.14: Bifurcating pseudo-Lorenz attractor from equations 3.11, with $\rho = 20$, $\sigma = 10$ and $\beta = 8/3$. The parameter $B$ was raised to 20 for this plot, to enhance the spiralling motion near the fixed point $P^+$. Spiralling is also evident, but less pronounced, at $\rho = 10$ for lower values of $B$.
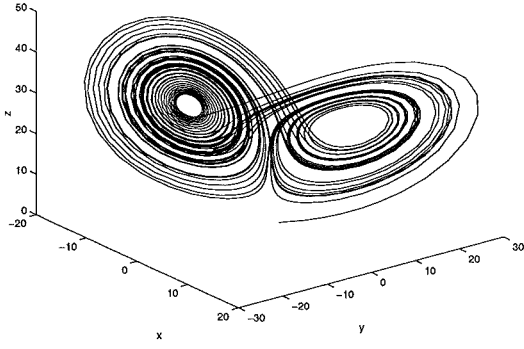
Figure 3.15: Lorenz attractor from equations 3.1, with $\rho = 28$, $\sigma = 10$ and $\beta = 8/3$
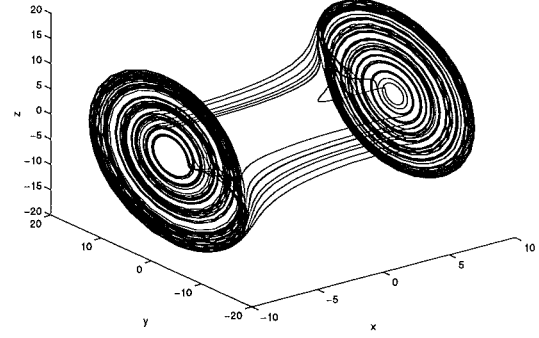


Figure 3.16: Bifurcating pseudo-Lorenz attractor from equations 3.11, with $\rho = 28$, $\sigma = 10$ and $\beta = 8/3$

## 3.4 Developments of Lorenz Attractor

### 3.4.1 Oppositely-directed Pseudo-Lorenz attractor

The direction of spiralling can be changed by a simple modification of the slow subsystem. Figure 3.17 shows a version of equations 3.3 with the flows on the stable branches of the slow subsystem modified so that they spiral in opposite directions.

This is done simply by replacing the $h$ equations in 3.4 with

$$
\begin{aligned}
h_x &= 0.1x + y \\
h_y &= 0.1y - x
\end{aligned} \tag{3.14}
$$

### 3.4.2 A Pseudo-Lorenz attractor with three branches in the slow subsystem

As with earlier examples, we can combine switches to produce more complicated attractors. This system is analogous to that of equations 3.3, but uses a ZZ-switch to produce a Lorenz-like attractor with three lobes instead of two. The equations are

$$
\begin{aligned}
\dot{x} &= (z+1)z(z-1)(z-2)f_x - (z+2)z(z-1)(z-2)g_x + (z+2)(z+1)(z-1)(z-2)f_x \\
&\quad -(z+2)(z+1)z(z-2)g_x + (z+2)(z+1)z(z-1)f_x \\
\dot{y} &= (z+1)z(z-1)(z-2)f_y - (z+2)z(z-1)(z-2)g_y + (z+2)(z+1)(z-1)(z-2)f_y \\
&\quad -(z+2)(z+1)z(z-2)g_y + (z+2)(z+1)z(z-1)f_y \\
\varepsilon\dot{z} &= 0.4((2-z)z(2+z)(z-mx+1)(z-mx-1) - \varepsilon cz)
\end{aligned} \tag{3.15}
$$

where

$$
f_x = 0.1x - y
$$
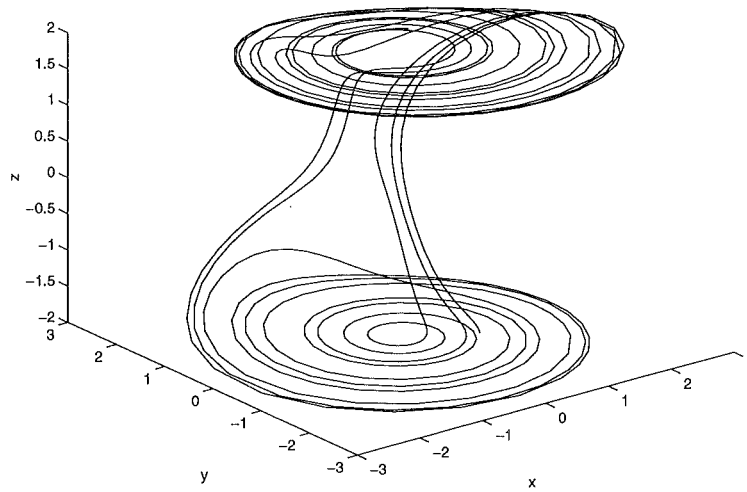
Figure 3.17: Oppositely-directed Pseudo-Lorenz attractor

$$
\begin{aligned}
f_y &= 0.1y + x \\
g_x &= -x \\
g_y &= -y
\end{aligned}
\tag{3.16}
$$

and figure 3.18 shows the attractor generated by them.
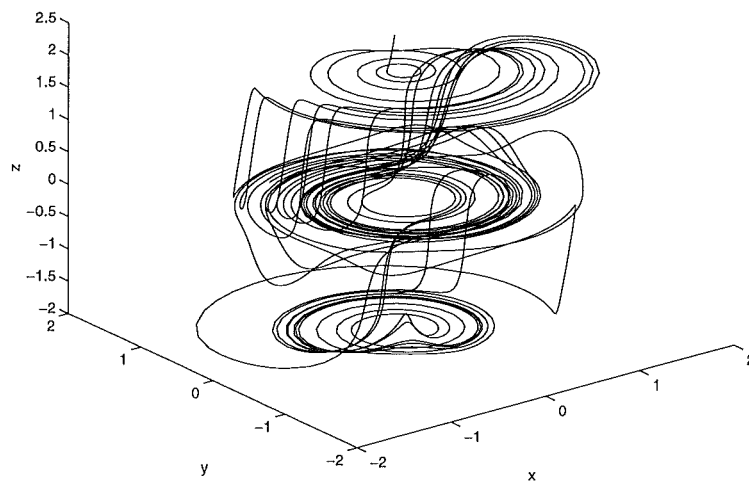
Figure 3.18: Pseudo-Lorenz attractor with three branches in the slow subsystem, from equations 3.15

# Chapter 4

# Chua's circuit

Chua's circuit is not just a mathematical model, but an actual electronic circuit, the first physical object for which chaotic behaviour was proven analytically, numerically and experimentally.

In the original circuit, Chua used a piecewise linear function as the nonlinear component of the system [Chu92]. In this thesis, this function is replaced with a cubic polynomial in one variable, following the example given in [PWH96]. This function has the advantage of being analytic, while the system containing it still exhibits all the same phenomena as the original system developed by Chua.

The dynamical system inherent in Chua's circuit is in a sense simpler than the Lorenz system, as it has only one nonlinear component, with one variable. However, the Chua system exhibits a richer array of behaviour than the Lorenz system, encompassing most of the interesting dynamical phenomena observed in the Lorenz system, and others that have so far not been observed in that system.

## 4.1  Chua Equations

The Chua system is described by the following equations

$$\dot{x} = k\alpha[y - g(x)]$$
$$\dot{y} = k(x - y + z)$$
$$\dot{z} = k(-\beta y - \gamma z)$$

where $\alpha$, $\beta$ and $k$ are constants and $g(x) = ax^3 + cx$ is the nonlinear function that replaces the original piecewise linear function. The system is invariant under the transformation $(x, y, z) \rightarrow (-x, -y, -z)$.

The origin is a fixed point for all parameter values, and there are two other fixed points for $a \neq 0$, with coordinates

$$x = \pm\sqrt{(\frac{\gamma}{\gamma + \beta} - c)/a}$$
$$y = \pm\frac{\gamma}{\gamma + \beta}\sqrt{(\frac{\gamma}{\gamma + \beta} - c)/a}$$
$$z = \frac{\beta}{\gamma + \beta}\sqrt{(\frac{\gamma}{\gamma + \beta} - c)/a}$$
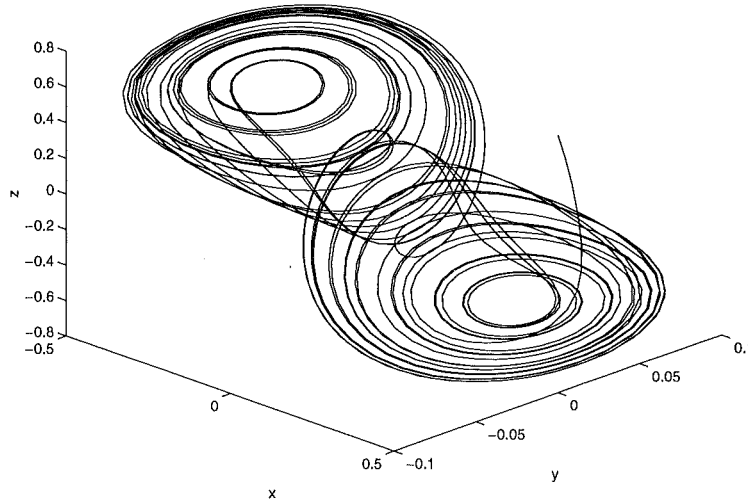
Figure 4.1: Double-scroll Chua's attractor from equations 4.1, with $\alpha = 10$, $\beta = 16$, $\gamma = 0$, $a = 1$, $c = -0.143$ and $k = 1$

Figure 4.1 shows the most famous of the attractors generated by equations 4.1, the Double-scroll Chua's attractor. [Mad93]

Other attractors generated by this system are shown in [CWHZ93a], and [CWHZ93b]. Further figures are shown in [PWH96], with corresponding information on the eigenvalues of the linearized flows around the fixed points.

## 4.2 An equivalent of the double-scroll Chua's attractor using the modified Deng scheme

A small modification of equations 3.3 serves to reproduce the features of the Double-Scroll Chua Attractor. For this attractor, the fixed points $P^+$ and $P^-$ are qualitatively similar to the corresponding fixed points of the Lorenz system. In both systems, $P^+$ and $P^-$ have one-dimensional stable manifolds and two-dimensional unstable manifolds defined by complex conjugate eigenvalues. At the origin, however, the eigenvalues of the linearized flow corresponding to the stable manifold are both real in the Lorenz system, but are complex conjugates in the Chua system. These features of the fixed points are illustrated in figure 4.2

This difference can readily be modelled using the modified Deng scheme. Loosely speaking, a degree of "spin" is imparted to trajectories passing from one stable branch of the slow subsystem to the other, in addition to the spiral flows on the branches themselves.

The equations

$$\dot{x} = (z+2)zf_x + (z+2)(2-z)g_x - (2-z)zf_x$$
$$\dot{y} = (z+2)zf_y + (z+2)(2-z)g_y - (2-z)zf_y$$
$$\varepsilon\dot{z} = e(2+z)(2-z)(z-mx) - \varepsilon z \tag{4.1}$$

where

$$f_x = ax - by$$

47
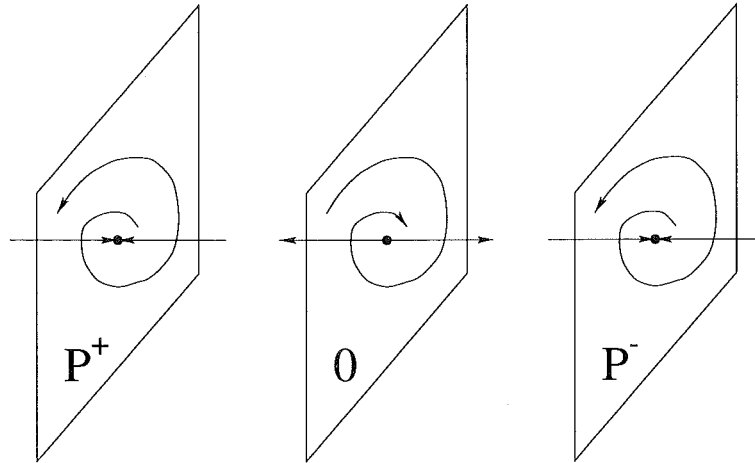
Figure 4.2: Fixed points of the Chua system for $\rho = 28$

$$\dot{f}_y = ay + bx$$
$$g_x = -cx - dy$$
$$g_y = -cy + dx$$

(4.2)

describe such a system. Note that this system is almost identical to that of equations 3.3. The only significant differences are in the functions $g_x$ and $g_y$, where extra terms have been added to change the nature of the stable manifold at the origin. Note that for $d = 0$, and with appropriate values for other variables, the behaviour of the system in 4.1 will reduce to that of the Lorenz Attractor.

Figure 4.3 shows this system, with values for parameters selected to emulate the Double-Scroll attractor. Figures 4.4 and 4.5 show other attractors generated by equations 4.1. These equations exhibit a wide variety of behaviour corresponding to that of the actual Chua system.
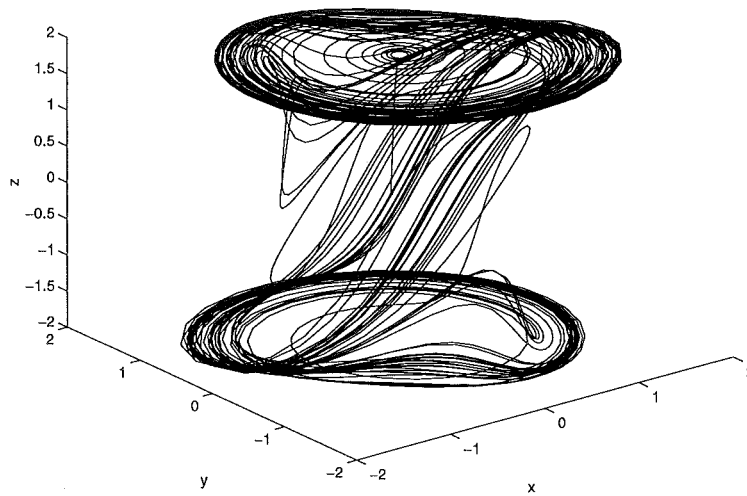
Figure 4.3: Pseudo-Chua double scroll attractor from equations 4.1, with $a = 0.05$, $b = 0.8$, $c = 0.4$, $d = 1.2$, $e = 0.3$, $m = 1$ and $\varepsilon = 0.1$
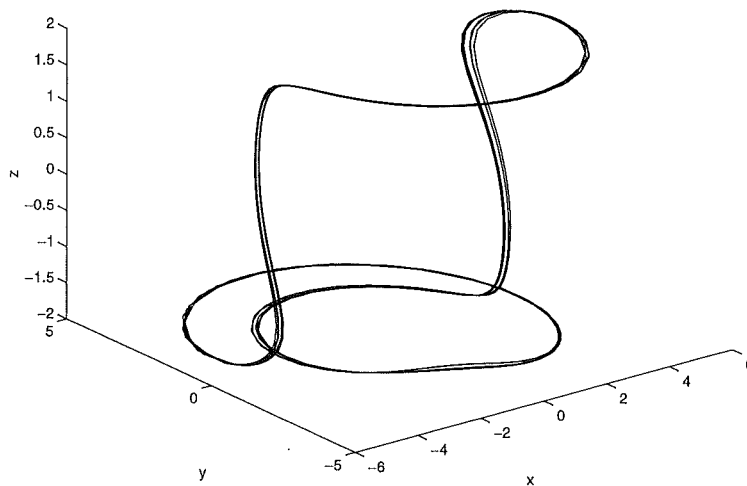


Figure 4.4: Pseudo-Chua attractor from equations 4.1, with $a = 0.09$, $b = 0.905$, $c = 0.6$, $d = -1.2$, $e = 0.1$, $m = 1$ and $\varepsilon = 0.1$

49
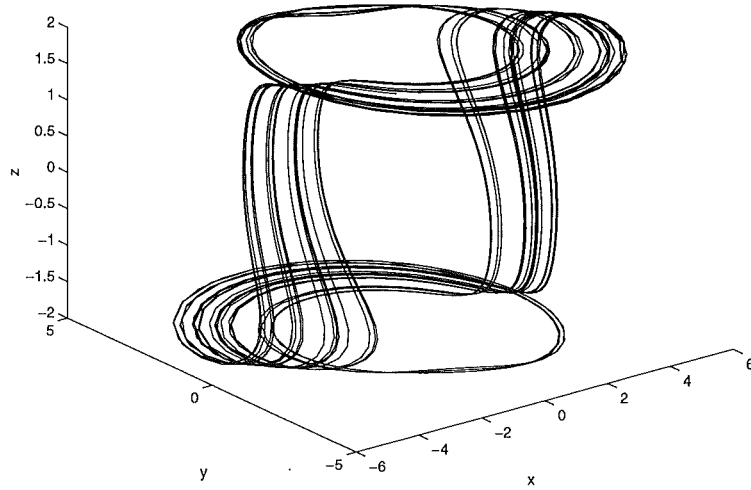
Figure 4.5: Pseudo-Chua attractor from equations 4.1, with $a = 0.097$, $b = 0.905$, $c = 0.6$, $d = -1.2$, $e = 0.1$, $m = 1$ and $\varepsilon = 0.1$

# Chapter 5

# Conclusion

The method developed by Deng, and extended in this thesis, is capable of reproducing the qualitative behaviour of many dynamical systems, including such well-studied systems as the Lorenz attractor and Chua's circuit. Systems developed under the Deng method have the advantage of a modular structure of largely independent subsystems, allowing for easy modification and extension, including extension to systems of higher dimension than those discussed in this thesis.

These features would be especially useful for modelling applications, in which a system must be developed to match observed dynamical behaviour. The Deng scheme allows construction of models based on limited amounts of qualitative information. The pseudo-Lorenz system defined in equations 3.3, for example, could have been developed from the observed behaviour of the Lorenz attractor, without reference to the Lorenz equations. The extension to a second pseudo-Lorenz model in equations 3.11 that included bifurcation properties could likewise have been developed from observation alone. It is conceivable that the Deng scheme could be automated, to produce a heuristic that would take a collection of data and convert it into a set of dynamical equations.

A possible direction for future research would involve the use of the Deng scheme as a diagnostic tool for examining the behaviour of other systems. The behaviour of the systems developed under the scheme is well understood, and comparing dynamical systems with comparable Deng systems might serve to highlight features of the former that were not previously evident. For example, it has been observed that all known dynamical behaviour of the Lorenz equations has also been observed in Chua's circuit [PWH96]. An examination of pseudo-Chua model in equations 4.1, moreover, reveals that it is a superset of the pseudo-Lorenz model of equations 3.3. With one parameter set to zero, the pseudo-Chua model reduces to the pseudo-Lorenz one. Knowing whether this is significant would require a more rigorous understanding of the connection between Deng systems and the systems they mimic.

# Appendix A

# Acknowledgements

I am grateful for the assistance of my supervisor Dr Mark Hickman at all stages of my work on this thesis.

Thanks are also due to my wife and family for their patience and support.

# Appendix B

# MATLAB Scripts

Mathwork's Inc.'s MATLAB software (version 5.1) was used extensively to generate pictures for this thesis. It is a matrix-based interpreted programming language, widely used for mathematical and scientific computing. MATLAB includes a series of commands for solving initial value problems such as those involved in plotting trajectories in the systems of equations discussed in this thesis.

Most of the trajectory plots in this thesis were generated using the `ode15s` command, which uses a backward-difference method with variable step size to solve differential equations. Generally speaking, during discretization it uses higher order derivatives to calculate a discretization error, and adjusts the step size accordingly. This allows small steps to be taken where necessary, while still taking larger steps where possible for speed. The backward difference method used by `ode15s` will solve stiff problems, and is often faster than methods used for solving non-stiff systems.

This appendix discusses the two MATLAB scripts, or m-files, used to generate figure 3.4. The first script, `PseudoLorenz.m`, sets an initial point $(x0, y0, z0)$ from which to begin calculations, and defines values for the parameters $c, m$, and $\varepsilon$. These values are collected into a single vector `q0`.

This vector is provided as an argument to the `ode15s` command, along with initial and final values for the time variable `t` that parameterizes the trajectory, and the name of the second m-file, `PseudoLorenzEqn.m`, in which the system of equations is defined. This second m-file is run repeatedly, once for each instant of time.

The two scripts are listed below, with discussion of their contents. Line numbers are not included in the actual m-files, but are added here for convenience of reference.

## B.1 PseudoLorenz.m

```
1. options=odeset('outputfcn','odephas3');

2.

3. t0 = 0;

4. tfinal=40;

5. tspan=[t0,tfinal];

6.
```

```
7. x0 = 0.5;

8. y0 = 0.5;

9. z0 = 2;

10.

11. m=1.543;

12. epsilon = 0.1;

13. c=1;

14.

15. q0 = [x0,y0,z0,m,epsilon,c]';

16. [t,q] = ode15s('PseudoLorenzEqn',tspan,q0,options);

17.

18. plot3(q(:,1),q(:,2),q(:,3))

19.

20. xlabel('x')

21. ylabel('y')

22. zlabel('z')
```

line 1 uses the `odeset` command to set options for the ODE solver `ode15s`; in this case it specifies the function `odephas3.m` (supplied with MATLAB) for rendering output as graphics, and stores this setting in a variable `options`.

Lines 3- 5 set up a vector variable `tspan`, containing beginning and end times for the integration.

Lines 7- 9 set the initial point for the integration. A trajectory will be plotted from this point.

Lines 11- 13 set values for some constants used in the system, and line 15 gathers initial co-ordinates and constants into one vector variable q0, to be passed to `ode15s`.‘

Line 16 starts the ODE solver with variables `tspan`, q0 and `options`, using the equations defined in the other m-file, `PseudoLorenzEqn.m`. For each instant of time t, `ode15s` returns a co-ordinate vector q indicating the current location of the trajectory being chased. Both time and location are recorded in a matrix, which the output function `odephas3.m` uses to plot the results as they are calculated.

Line 18 produces a final plot of the trajectory from the information generated by `ode15s`, and lines 20- 22 label the axes.

## B.2 PseudoLorenzEqn.m

```
1.  function qp = PseudoLorenzEqn(t,q)
2.
3.  t
4.
5.  x=q(1,1);
6.  y=q(2,1);
7.  z=q(3,1);
8.  m=q(4,1);
9.  epsilon=q(5,1);
10. c=q(6,1);
11.
12. fx = 0.1*x-y;
13. fy = 0.1*y+x;
14.
15. gx = -x;
16. gy = -y;
17.
18. xp = (z+2)*z*fx + (z+2)*(2-z)*gx - (2-z)*z*fx;
19. yp = (z+2)*z*fy + (z+2)*(2-z)*gy - (2-z)*z*fy;
20. zp = 0.1*((2+z)*(2-z)*(z - m*x) - epsilon*c*z)/epsilon;
21.
22. qp(1,1) = xp;
23. qp(2,1) = yp;
24. qp(3,1) = zp;
25. for n = 4:6
26.    qp(n,1) = 0;
27. end
```

Line 1 states that this m-file is a function, and that the output of the function will be given by the variable qp.

Line 3 prints the current time t in the MATLAB window. Although this slows down the running of the script, it is useful for debugging purposes.

Lines 5- 10 extract values from the input vector q as variables. This step is not strictly necessary either, as the various parameters and constants could be referred to directly as components of q. However, this method makes the following equations more readable, and easy to transfer to other programs by a direct cut-and-paste operation.

Lines 12- 20 contain the equations describing the system. The derivatives $\dot{x}$, $\dot{y}$ and $\dot{z}$ are represented by the variables xp, yp and zp.

Finally, lines 22- 27 set up the output vector qp, containing the derivative information to be used by ode15s. Since the ODE solver expects a vector of the same size as the input vector q, the output is 'padded' with zeros in all but the first three components.

# Bibliography

[AP90]      D.K. Arrowsmith and C.K. Place. *An introduction to Dynamical Systems*. Cambridge University Press, Cambridge, 1990.

[Chu92]     L. O. Chua. The genesis of chua's circuit. *Archiv für Elektronik und Übertragungstechnik*, 46(4):250–257, 1992.

[CWHZ93a]   L. O. Chua, C. W. Wu, A. Huang, and G.Q. Zhong. A universal circuit for studying and generating chaos, part i: Routes to chaos. *IEEE Transactions on Circuits and Systems -I: Fundamental Theory and Applications*, 40(10):732–744, 1993.

[CWHZ93b]   L. O. Chua, C. W. Wu, A. Huang, and G.Q. Zhong. A universal circuit for studying and generating chaos, part ii: Strange attractors. *IEEE Transactions on Circuits and Systems -I: Fundamental Theory and Applications*, 40(10):745–761, 1993.

[Den93]     B. Deng. A mathematical model that mimics the bursting oscillations in pancreatic $\beta$-cells. *Mathematical Biosciences*, 119(2):241–250, 1993.

[Den94]     B. Deng. Constructing homoclinic orbits and chaotic attractors. *International Journal of Bifurcation and Chaos*, 4(4):823–841, 1994.

[GH83]      J. Guckenheimer and P. Holmes. *Nonlinear Oscillations, Dynamical Systems, and Bifurcations of Vector Fields*, volume 42 of *Applied Mathematical Sciences*. Springer-Verlag, New York, 1983.

[Gle94]     P. Glendinning. *Stability, instability and chaos: an introduction to the theory of nonlinear differential equations*. Cambridge University Press, Cambridge, 1994.

[Mad93]     R. Madan. *Chua's Circuit: A Paradigm for Chaos*. World Scientific, Singapore, 1993.

[PWH96]     L. Pivka, C. W. Wu, and A. Huang. Lorenz equation and chua's equation. *International Journal of Bifurcation and Chaos*, 6(12B):2443–2489, 1996.

[Rin85]     J. Rinzel. *Ordinary and Partial Differential Equations*, pages 304–316. Springer-Verlag, New York, 1985.

[Rös76]     O.E. Rössler. Chaotic behaviour in simple reaction systems. *Zeitschrift Naturforsch*, 31A:259–264, 1976.

[Shi70]     L.P. Shil'nikov. A contribution to the problem of the structure of an extended neighbourhood of a rough equilibrium state of saddle-focus type. *Math. USSR-Sb.*, 10:91–102, 1970.

[SR]        L.F. Shampine and M.W. Reichelt. The MATLAB ODE suite.